Skeletal muscle-specific overexpression of miR-486 limits mammary tumor-induced skeletal muscle functional limitations

Ruizhong Wang,[1] Brijesh Kumar,[1] Emma H. Doud,[2] Amber L. Mosley,[2] Matthew S. Alexander,[3] Louis M. Kunkel,[4] and Harikrishna Nakshatri[1,2,5]

[1]Department of Surgery, Indiana University School of Medicine, Indianapolis, IN 46202, USA; [2]Department of Biochemistry and Molecular Biology, Indiana University School of Medicine, Indianapolis, IN 46202, USA; [3]Department of Pediatrics, Division of Neurology, University of Alabama at Birmingham and Children's of Alabama, Birmingham, AL 35294, USA; [4]Boston Children's Hospital, Harvard Medical School, Boston, MA 02115, USA; [5]Richard L Roudebush VA Medical Center, Indianapolis, IN 46202, USA

miR-486 is a myogenic microRNA, and its reduced skeletal muscle expression is observed in muscular dystrophy. Transgenic overexpression of miR-486 using muscle creatine kinase promoter (MCK-miR-486) partially rescues muscular dystrophy phenotype. We had previously demonstrated reduced circulating and skeletal muscle miR-486 levels with accompanying skeletal muscle defects in mammary tumor models. To determine whether skeletal muscle miR-486 is functionally similar in dystrophies and cancer, we performed functional limitations and biochemical studies of skeletal muscles of MMTV-Neu mice that mimic HER2+ breast cancer and MMTV-PyMT mice that mimic luminal subtype B breast cancer and these mice crossed to MCK-miR-486 mice. miR-486 significantly prevented tumor-induced reduction in muscle contraction force, grip strength, and rotarod performance in MMTV-Neu mice. In this model, miR-486 reversed cancer-induced skeletal muscle changes, including loss of p53, phospho-AKT, and phospho-laminin alpha 2 (LAMA2) and gain of hnRNPA0 and SRSF10 phosphorylation. LAMA2 is a part of the dystrophin-associated glycoprotein complex, and its loss of function causes congenital muscular dystrophy. Complementing these beneficial effects on muscle, miR-486 indirectly reduced tumor growth and improved survival, which is likely due to systemic effects of miR-486 on production of pro-inflammatory cytokines such as IL-6. Thus, similar to dystrophy, miR-486 has the potential to reverse skeletal muscle defects and cancer burden.

INTRODUCTION

MicroRNAs (miRNAs) have emerged as minimally invasive biomarkers of cancer progression and therapeutic response.[1,2] Plasma of patients with acute myeloid leukemia show low levels of miR-92a compared with healthy controls despite high levels of this miRNA in leukemic cells.[3] Similarly, sera of ovarian cancer patients show elevated levels of five miRNAs and decreased levels of three miRNAs compared with healthy controls.[4] In the sera of lung can-

cer patients, 28 miRNAs are missing, and 63 new miRNA species are detectable compared with healthy controls.[5] In fact, lower levels of circulating miR-486 in lung cancer patients are associated with poor outcomes.[6] In breast cancer patients, lower circulating levels of miR-486 have been reported by us and others,[1,7,8] which is consistent with the findings in animal models of mammary tumors.[9,10] Recently, we demonstrated that miR-486 is an estradiol-regulated microRNA, and decrease in its level in circulation is more severe in men with cancer compared with women with the same cancer type.[11] We further showed that the NF-κB inhibitor dimethylaminoparthenolide could restore circulating and skeletal muscle levels of miR-486, depending on the model system, and ameliorate cancer-induced functional limitations.[9,10] On the basis of these observations, we had proposed that circulating microRNAs, particularly those whose levels are reduced in cancer compared with healthy controls, likely reflect the systemic effects of cancer on microRNA biosynthesis and release from other organs such as skeletal muscle, and these microRNAs could be used as biomarkers of cancer-induced systemic effects.[9]

miR-486 is an integral part of a myogenesis signaling network that involves Pax7, MyoD, myostatin, and NF-κB.[12–14] miR-486 is essential for survival of cardiomyocytes, as it blocks PTEN to upregulate PI3K/AKT.[15] Loss of miR-486 is a major defect in Duchenne muscular dystrophy (DMD), and transgenic expression of miR-486 in muscle can rescue DMD phenotypes in animal models.[16,17] miR-486-knockout mice show severe defects in skeletal muscle, including increased levels of centralized myonuclei, elevated expression of miR-486 target genes such as metallothionine 2 (MT2), and metabolic defects.[18] The authors of this study concluded that miR-486 is an epigenetic regulator
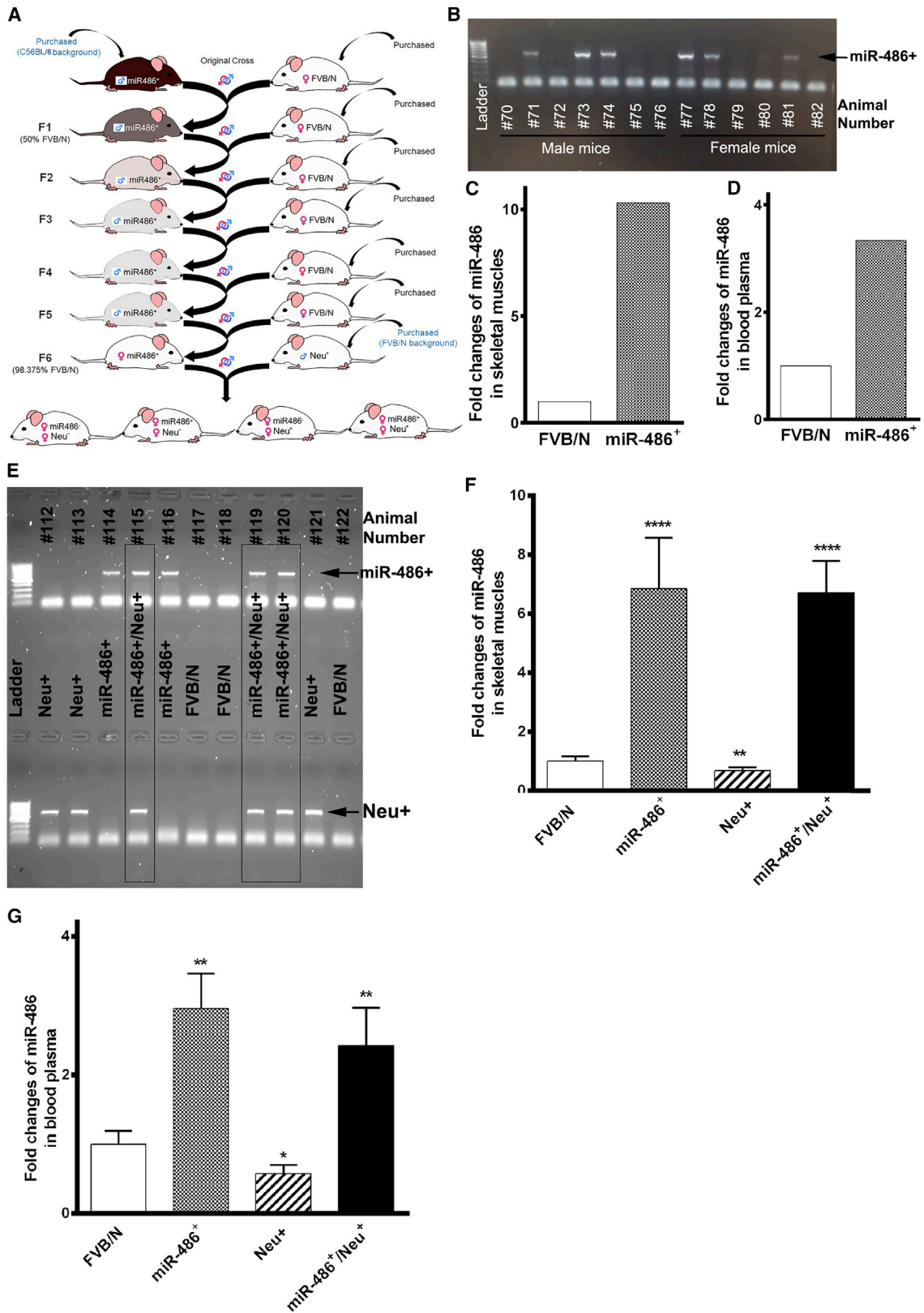
of DMD pathologies. With respect to cancer-associated skeletal muscle defects, miR-486 target MT2 levels are increased in cachectic, sarcopenic, and atrophic skeletal muscle.[19]

Given the known role of miR-486 in skeletal muscle biology and its deregulated skeletal muscle expression in both DMD and cancer, it is ideal to investigate whether cancer-induced skeletal muscle defects show similarity to skeletal muscle defects in DMD and, if so, whether restoration of skeletal muscle expression of miR-486 can overcome DMD-like skeletal muscle defects in cancer. To address these questions, we crossed MMTV-PyMT and MMTV-Neu transgenic mammary tumor models with MCK-miR-486 transgenic mice and characterized skeletal muscle. The MMTV-Neu (hereafter Neu+) model is a tumor model that represents a HER2-amplified intrinsic subtype of breast cancer, and animals with tumors survive to ∼220 days.[10] In contrast, MMTV-PyMT model (hereafter PyMT+) is an aggressive mammary tumor model with tumors resembling luminal B intrinsic subtype of breast cancer, and animals need to be sacrificed by ∼110 days. Although only 25% of breast cancer patients demonstrate classic cachexia-like symptoms, skeletal muscle defects leading to functional limitations and toxicity to chemotherapy are frequently observed in breast cancer patients.[20–22] Therefore, understanding skeletal muscle biology in breast cancer patients and developing appropriate therapeutic modalities is critical to improve quality of life. Although miR-486 overexpression failed to overcome skeletal muscle defects in PyMT+ mice, miR-486 reversed skeletal muscle defects in Neu+ mice. Skeletal muscle of Neu+ mice demonstrated elevated phosphorylation of the splicing factor SRSF10 (serine and arginine rich splicing factor 10) at the site typically phosphorylated by the SRSF protein kinases (SRPKs)[23] and Cdc2-like kinases such as CLK1-3,[24] pre-RNA processing factor hnRNPA0 (heterogeneous nuclear ribonucleoprotein A0) at the site phosphorylated by the MAP kinase-activated protein kinase 2 (MK2),[25] and lower phosphorylation of laminin subunit alpha2 (LAMA2) at the protein kinase A (PKA) consensus phosphorylation site. miR-486 overexpression abrogated all of these Neu+ tumor-induced alterations in the skeletal muscle. Skeletal muscle miR-486 controlled systemic inflammation as basal levels of several circulating cytokines such as CCL4, CXCL10, G-CSF, IL-4, IL-6, and TNF-α were lower in miR-486 transgenic mice compared with wild-type mice and in double-transgenic mice compared with tumor-bearing mice. Interestingly, skeletal muscle-enriched expression of miR-486 reduced tumor burden and improved survival of mice, suggesting that either miR-486 induced changes in systemic cytokines or reciprocal skeletal muscle-tumor interactions affecting skeletal muscle secretome have anti-tumorigenic effects.

RESULTS

Generation of animal models to study the influence of skeletal muscle miR-486 on cancer-induced functional limitations

Transgenic MMTV-Neu and MMTV-PyMT female mice in FVB/N background were used to characterize systemic impacts of mammary tumors in mouse model of breast cancer as described in previous studies.[9,10] Double-transgenic mice of miR-486+/Neu+ and miR-486+/PyMT+ in FVB/N background were generated to test the role of functional biomarker miR-486 in overcoming cancer-induced systemic effects. First, we backcrossed MCK-miR-486 transgenic mice in C57BL/6 background to FVB/N background for six generations (Figure 1A). Genotype was monitored in each generation to ensure that miR-486 gene was not lost during backcrossing (Figure 1B). Overexpression of miR-486 in skeletal muscles and resulting elevation of its levels in plasma were determined after six-generation backcrossing (Figures 1C and 1D). Next, crossbreeding of female miR-486+ mice with male Neu+ mice in an FVB/N background enabled generation of four groups of mice: miR-486−/Neu− (FVB/N), miR-486+/Neu−, miR-486−/Neu+, and miR-486+/Neu+ mice (Figure 1A). Genotypes were characterized (Figure 1E), and overexpression of miR-486 in skeletal muscles and its elevated levels in plasma of double-transgenic mice were confirmed (Figures 1F and 1G). We did not observe an overexpression of miR-486 in the heart muscles of miR-486+ and miR-486+/Neu+ mice compared with control mice (Figure S1). Only female transgenic mice were used for further evaluation of tumor progression (tumor onset time, size, and volume), body composition alteration (body weight, body fat, lean mass, body free water, and total water), function limitations (grip strength and rotarod performance), and ex vivo muscle contraction force studies.

miR-486 reduces Neu+ tumor-induced functional limitation of skeletal muscle

Reduction of grip strength from front limbs was observed in tumor-bearing Neu+ mice compared with wild-type mice, as previously reported.[10] At 24 weeks post-birth, Neu+ mice had 191 ± 3.99 g grip strength, which was significantly lower than the 223 ± 2.42 g grip strength demonstrated by age-matched FVB/N female mice (Figure 2A). Double-transgenic mice displayed a grip force of 219 ± 4.16 g, suggesting the ability of miR-486 to reverse the effects of tumors on grip strength. Similarly, miR-486-mediated attenuation of grip strength loss was maintained at 28 weeks post-birth, although the effects were not as apparent as at 24 weeks (Figure 2A). Overexpression of miR-486 did not change grip strength in non-tumor-bearing animals (Figure 2A). In the rotarod motor function test, Neu+ mice walked on rod approximately 45 ± 9.8 s, compared with control mice, which were on the rod for 102 ± 8.0 s. Double-transgenic mice were on the rod for 76 ± 6.4 seconds, which was

Figure 1. Animal model creation

(A) Male MCK-miR-486 mouse in C57BL/6 background was backcrossed with female FVB/N mouse for six generations to obtain MCK-miR-486 mouse in FVB/N background. Resulting miR-486 transgenic female was crossed with MMTV-Neu+ male mice in FVB/N background to generate four groups of mice in FVB/N background: FVB/N, miR-486+, Neu+, and miR-486+/Neu+ mice. (B) Confirmation of miR-486 transgene in FVB/N mice during backcrossing. (C and D) Verification of miR-486 expression in skeletal muscles and plasma after six generations of backcrossing; n = 2 per group. (E) Confirmation of miR-486 and Neu transgenes in miR-486+/Neu+ double-transgenic mice. (F and G) Verification of transgenic miR-486 expression in skeletal muscles and plasma; (p < 0.05) n = 5 per group. *Significance by comparison with FVB/N group.
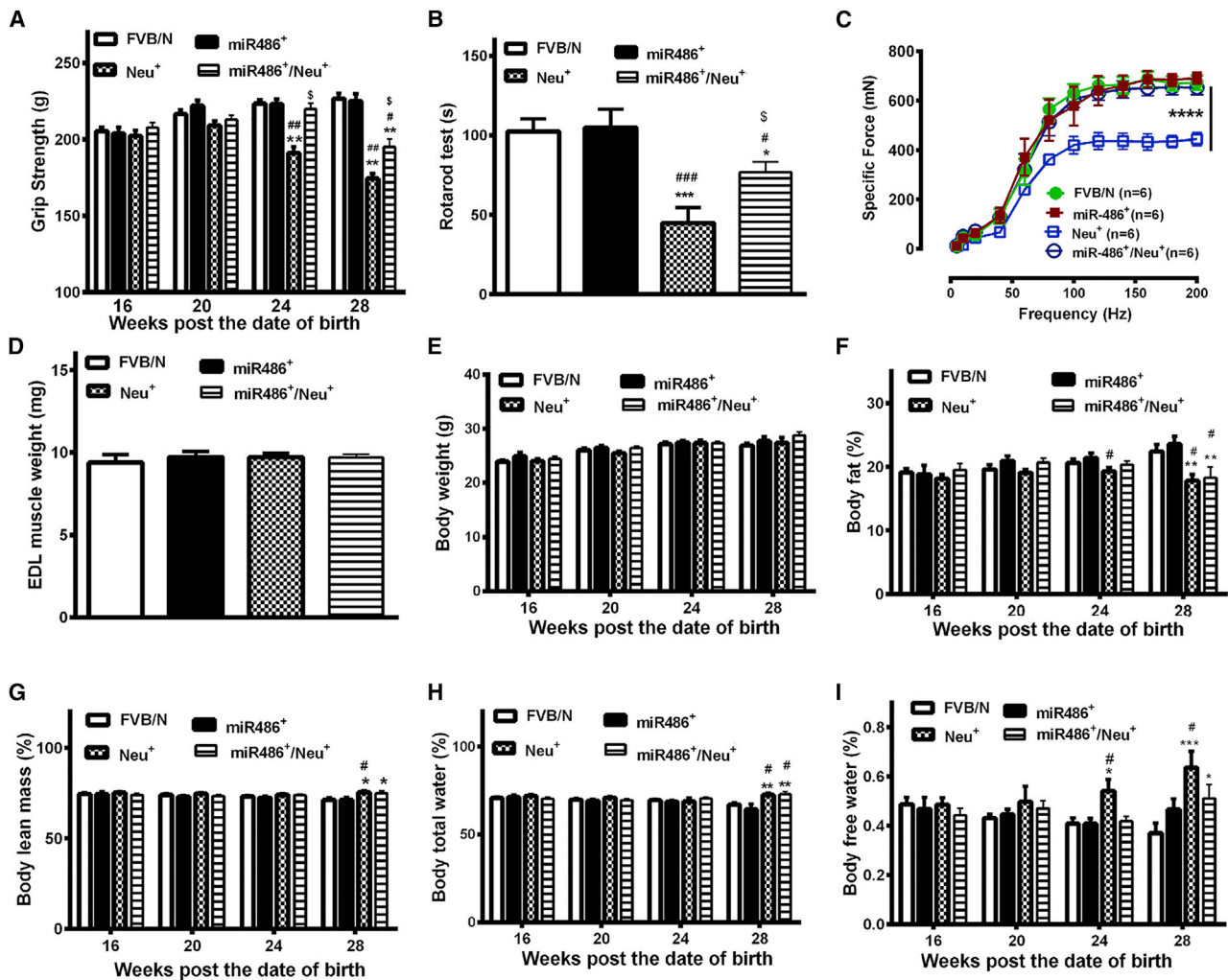
Figure 2. Functional limitation and body composition studies

(A) miR-486 overexpression restored grip strength force in Neu+ mice (n =12/group; p= 0.0037). (B) Reduced rotarod performance in Neu+ mice was restored upon overexpression of miR-486 in skeletal muscle (n =12/group; p < 0.0001). (C) Skeletal muscle of Neu+ mice displayed lower contraction force compared with age- and sex-matched controls (p < 0.0001), and miR-486 overexpression restored contraction force (n = 6). (D) EDL muscle weight (n = 6 per group). (E) Mouse body weight (n = 12). (F) Reduced body fat percentage in Neu+ mice with tumors (p = 0.0036; n = 12 per group). (G) Body lean mass within observation period (n = 12 per group). (H) Body total water (n = 12 per group). (I) Body free water elevated in Neu+ tumors was reversed upon overexpression of miR-486 (p < 0.001; n = 12 per group). *Significance by comparison with FVB/N group. #Significance by comparison with miR-486+ group. $Significance by comparison with Neu+ group.

significantly higher compared with Neu+ mice (p < 0001), indicating the ability of miR-486 to improve motor function in tumor-bearing mice (Figure 2B). Rotarod performance of FVB/N mice overexpressing miR-486 was similar to that of wild-type mice (104 ± 11.5 s). These results imply that miR-486 has the ability to prevent cancer-associated muscle dysfunction *in vivo*, similar to previously reported ability of miR-486 to reverse muscular dystrophy phenotypes.[16,17]

As a complementary to *in vivo* studies, we measured muscle contraction force of skeletal muscle *ex vivo* from all four groups of mice. Extensor digitorum longus (EDL) muscle from Neu+ mice showed significantly lower contraction force compared with EDL from

FVB/N mice or the double-transgenic mice (Figure 2C). Two-factor (miR-486+ and Neu+) ANOVA showed that miR-486+ and Neu+ had strong interactions (p < 0.0001). miR-486+ had a significant impact on contraction force of skeletal muscle isolated from double-transgenic mice compared with Neu+ mice (p < 0.0001). However, these differences in contraction force are unlikely due to differences in weights of EDL muscles, as muscle weight was similar in all four groups (Figure 2D).

miR-486 delays Neu+ mammary tumor-induced loss of body fat

It is well documented that cancer causes changes in body compositions with consequential effects on skeletal muscle function.[21]
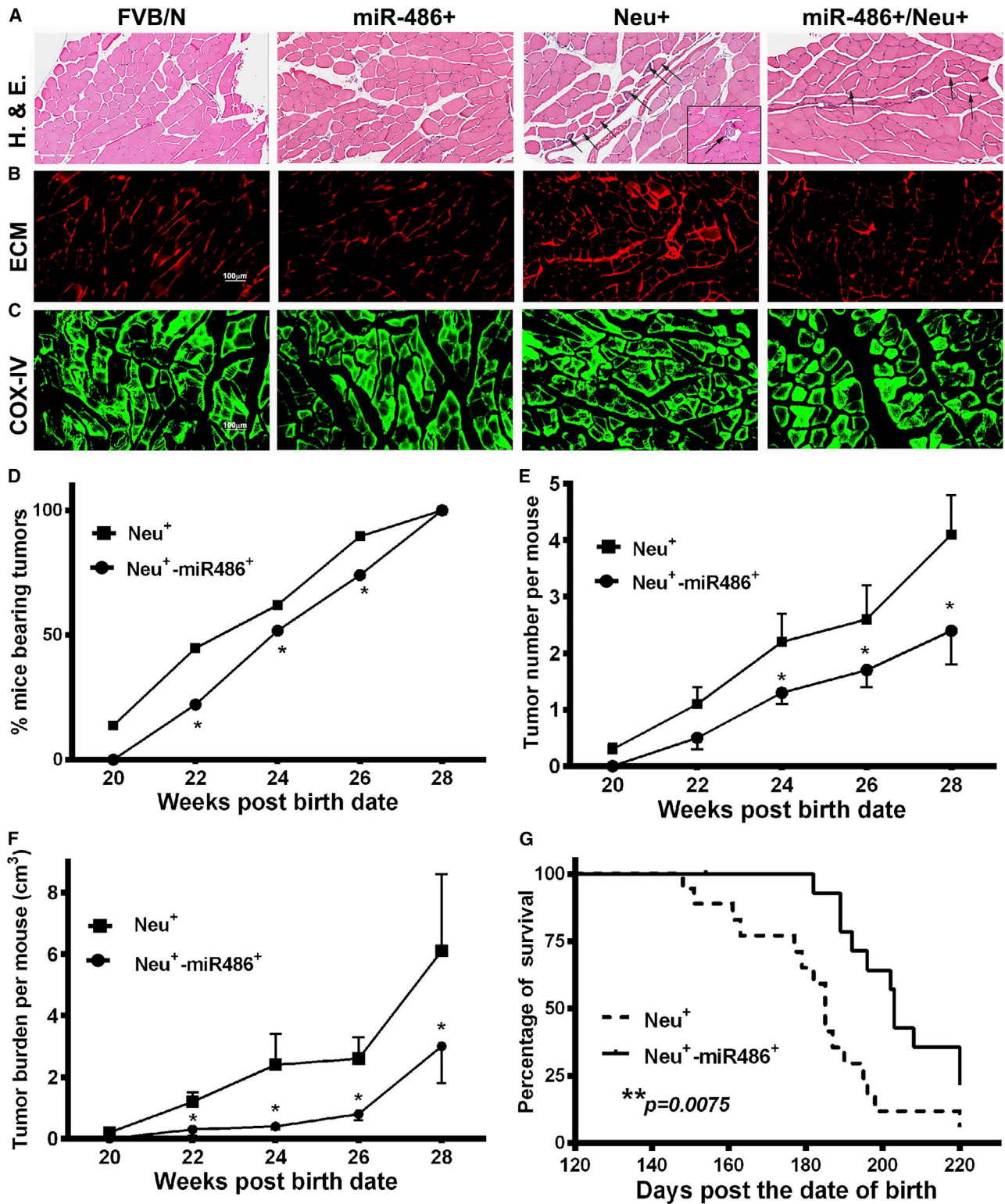
Figure 3. The effects of Neu+ and miR-486 overexpression on muscle structure and tumor burden

(A) Enhanced muscle shrinkage (arrows) and degeneration (insert) observed in Neu+ mice were attenuated upon overexpression of miR-486 (n = 6 per group). (B) Over-expression of miR-486 ameliorated ECM accumulation in skeletal muscles of Neu+ mice (n = 6 per group). (C) Overexpression of miR-486 had no effect on mitochondrial

(legend continued on next page)

Therefore, we next tested whether miR-486 overexpression affects mammary tumor-associated body composition changes. Four groups of mice did not differ in their body weight (Figure 2E). However, significant reduction of body fat was observed in Neu+ mice by 24 weeks, and this reduction in body fat was delayed until 28 weeks of age in miR-486+/Neu+ mice (Figure 2F). miR-486 had no effect on Neu+ tumor-induced changes in body lean mass (Figure 2G) and total body water (Figure 2H). However, miR-486 overexpression reversed the enhancements of body free water in Neu+ tumor-bearing mice (Figure 2I). Interestingly, two-factor (miR-486+ and Neu+) ANOVA showed that only Neu+ had significant a impact on mouse body compositions (body fat, body free water, body total water, and body lean mass; $p < 0.05$). The observation that miR-486 did not have a significant impact on lean mass is consistent with observation of a lack of effect of miR-486 on EDL muscle weight in mice with or without mammary tumors. Thus, muscle-specific overexpression of miR-486 may indirectly reverse few but not all cancer-induced body composition changes.

miR-486 protects skeletal muscle structural integrity in Neu+ mice

To examine whether the differences noted above regarding muscle contraction force and functional limitations among the four groups correlate with skeletal muscle structural changes, H&E-stained cross sections of mouse quadriceps were analyzed blindly by a pathologist. We did not observe significant difference in cross myofiber area among four groups; the average area was 5,548 ± 385, 6,124 ± 635, 5,254 ± 408, and 5,966 ± 327 μm^2 per cross myofiber in FVB/N, miR-486+, Neu+, and miR-486+/Neu+ mice, respectively. However, similar to our previous report,[10] there was significant myofiber degeneration (Figure 3A, insert) and myofiber shrinkage (arrows) in Neu+ mice (Figure 3A). These defects were significantly lower in double-transgenic mice (Figure 3A). The number of shrunk and degenerative myofibers were 3.1 ± 0.2, 2.7 ± 0.3, 11.38 ± 2.3, and 4.6 ± 1.2 cells/mm^2 cross-sectional area in FVB/N, miR-486+, Neu+, and miR-486+/Neu+ mice, respectively. Extracellular matrix (ECM) accumulation in skeletal muscles impedes muscle contraction by increasing stiffness of the ECM network and the nonfunctional fibrotic part,[26] which is a critical factor that contributes to muscle dysfunction in cancer-associated cachexia and function limitations.[10,27] Skeletal muscle of Neu+ mice displayed significant deposition of ECM (Figure 3B), which occupied 22.4% ± 2.4% of muscle section area, compared with 10.5% ± 1.1%, 9.2% ± 0.7%, and 12.1% ± 1.2% in FVB/N, miR-486+, and miR-486+/Neu+ mice, respectively. The present observation is consistent with our previous report,[10] and this ECM accumulation was not observed in double-transgenic mice (Figure 3B). However, no significant differences in mitochondria contents in skeletal muscle, as measured using COX-IV staining, were noted

among the four groups of mice (Figure 3C). The occupied area by COX-IV labeling over sectioned muscle were 26.4% ± 3.0%, 26.3% ± 2.3%, 30.6% ± 3.9%, and 27.8% ± 2.3% in FVB/N, miR-486+, Neu+, and miR-486+/Neu+ mice, respectively.

miR-486 inhibits mammary tumor occurrence and tumor growth in Neu+ mice

Skeletal muscle is considered a secretory organ, and factors released from skeletal muscle such as irisin display paracrine effects on metabolic organs and anti-tumor activity.[28,29] miR-486 secreted by skeletal muscle can itself have anti-tumor effects in a paracrine manner, as tumor-suppressor function of this microRNA has been reported.[2] For example, downregulation of miR-486 in non-small-cell lung cancer promotes tumor growth and metastasis,[1,30] and its overexpression inhibits tumor cell proliferation and invasion.[31] Consistent with this possibility, tumor phenotype in double-transgenic mice was different compared with Neu+ mice (Figure 3D). By 20 weeks, approximately 14% of Neu+ mice developed mammary tumor, whereas no tumors were observed in miR-486+/Neu+ mice. Approximately 44%, 62%, 89%, and 100% of Neu+ mice had tumors at 22, 24, 26, and 28 weeks post-birth. In case of double-transgenic mice, approximately 22%, 51%, 71%, and 100% of mice developed tumors at 22, 24, 26, and 28 weeks post-birth, respectively (Figure 3D). When the tumors were counted, we found that double-transgenic miR-486+/Neu+ mice had fewer tumors than Neu+ mice during the period of observation (Figure 3E). These results indicate that overexpression of miR-486 *in vivo* inhibits mammary tumor occurrence. It is more obvious that miR-486 inhibits mammary tumor growth, as tumor burden per mouse was approximately 0, 0.5, 1.3, 1.7, and 2.4 cm^3 at 20, 22, 24, 26, and 28 weeks post-birth, respectively, in double-transgenic mice compared with the tumor burden per mouse of 0.3, 1.1, 2.2, 2.6, and 4.1 cm^3, respectively, in Neu+ mice (Figure 3F). As a consequence of effects on tumor characteristics as well as beneficial effects on skeletal muscle function, double-transgenic mice survived longer than Neu+ mice (Figure 3G). These results suggest that restoring miR-486 expression in skeletal muscle has multiple beneficial effects, including improving skeletal muscle function and delaying tumor growth. However, these effects of skeletal muscle-derived miR-486 on tumor growth properties are unrelated to miR-486 levels in tumors, as we did not find any difference in miR-486 levels in tumors of Neu+ and miR-486+/Neu+ mice (Figure S1). Thus, there is no inadvertent expression of transgene in tumors of miR-486+/Neu+ mice.

miR-486 modulates molecular changes in skeletal muscles of Neu+ tumor-bearing mice

PTEN is one of the downstream targets of miR-486 in skeletal muscle.[15] Thus, the ability of miR-486 to improve myogenesis and

content as measured by COX-IV staining (n = 6 per group). (D) Overexpression of miR-486 in skeletal muscle delayed tumor onset in Neu+ mice ($p < 0.05$; n = 12 per group). (E) miR-486 overexpression reduced number of tumors per mouse ($p < 0.05$; n = 12 per group). (F) miR-486 overexpression in skeletal muscle resulted in smaller tumors ($p < 0.05$; n = 12 per group). (G) miR-486 overexpression increased survival rates of Neu+ mice ($p = 0.0075$; n = 12 per group). *Significance between Neu+ and miR-486+/Neu+ groups.
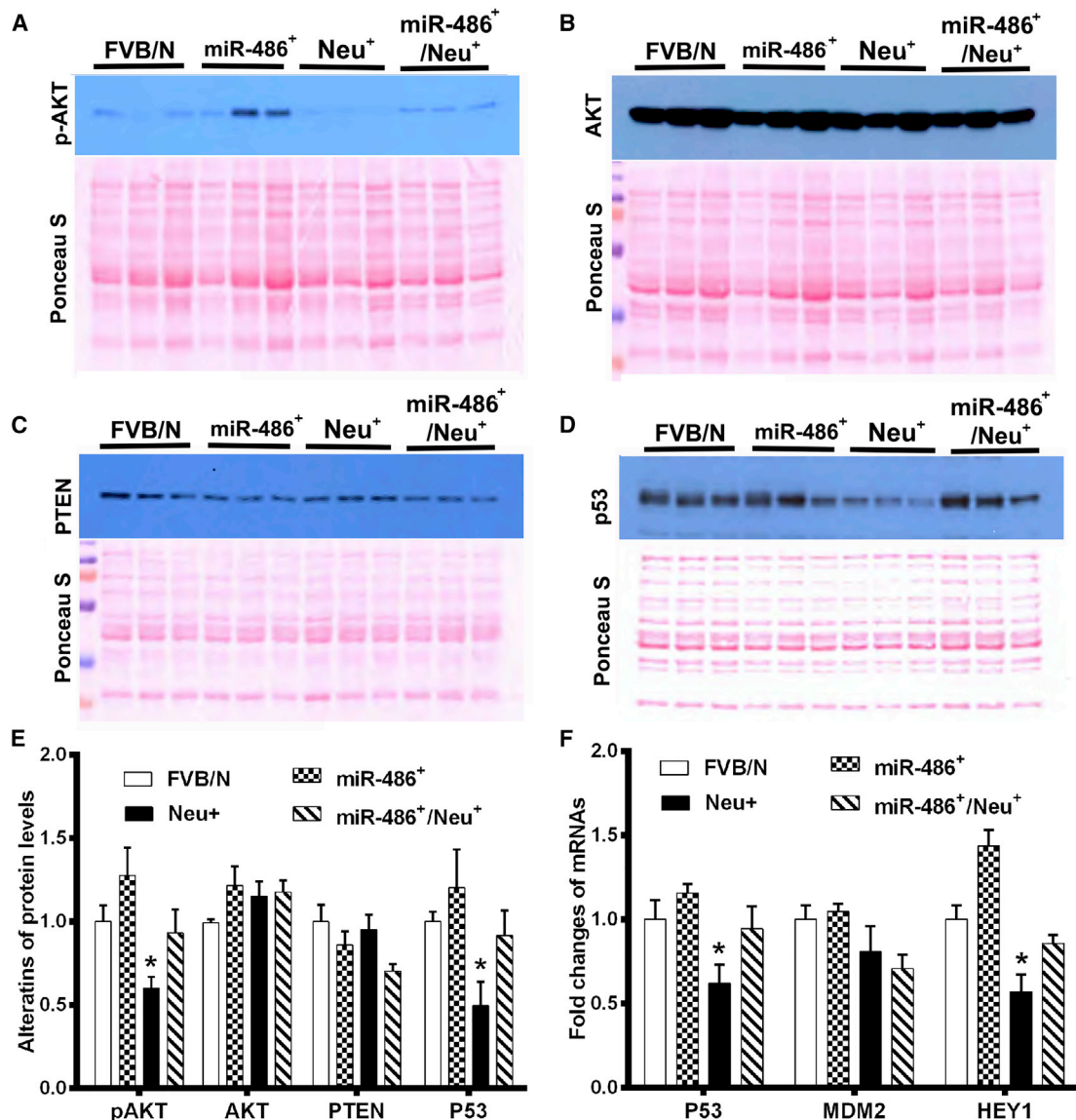
Figure 4. Molecular changes in skeletal muscle upon overexpression of miR-486

TA skeletal muscles were harvested at the end of behavioral tests (∼28 weeks old), stored at −80°C, and then processed for western blotting. Three samples per group derived from different animals were loaded and are presented in (A)–(D). There were four groups of mice: FVB/N, miR-486+, Neu+, and miR-486+/Neu+ mice. (A) miR-486 overexpression restores skeletal muscle active AKT levels in Neu+ mice (n = 9 per group), as measured by an antibody that recognizes phosphorylated S473. (B) miR-486 overexpression did not change the levels of total AKT in skeletal muscles (n = 9 per group). (C) PTEN protein levels in skeletal muscles of mice of four groups (n = 9 per group). (D) miR-486 reversed Neu+ tumor-induced loss of p53 in skeletal muscles (n = 9 per group). (E) Quantification of proteins p-AKT, AKT, PTEN, and p53 in skeletal muscles of mice by ImageJ ($p < 0.05$; n = 9 per group). (F) Down-regulation of *p53* and *Hey1* but not *Mdm2* mRNA in skeletal muscles of Neu+ mice and miR-486 reversed the effects of tumor on their expression ($p < 0.05$; n = 6 per group). *Significance by comparison with FVB/N group.

to restore muscle function in DMD models likely involves inactivation of PTEN and consequently activation of AKT.[15,16] To determine whether a similar miR-486-PTEN-AKT signaling axis is operational in our model system, we next examined phospho-AKT (S473) levels in skeletal muscle of animals in all four groups. As expected, phospho-AKT levels were lower in the skeletal muscle of Neu+ mice compared with control mice, although total AKT levels were not different

(Figures 4A and 4B). However, pAKT levels in double-transgenic mice were higher than in Neu+ mice, suggesting the ability of miR-486 to restore skeletal muscle pAKT levels. Unlike the previous reports on miR-486-PTEN axis in skeletal muscle,[15] the effect of overexpressed miR-486 on PTEN was modest (Figure 4C), suggesting that miR-486 targets other components of the PI3K-PTEN-AKT pathway to activate AKT *in vivo*. In this regard, as per the miRDB database,[32]
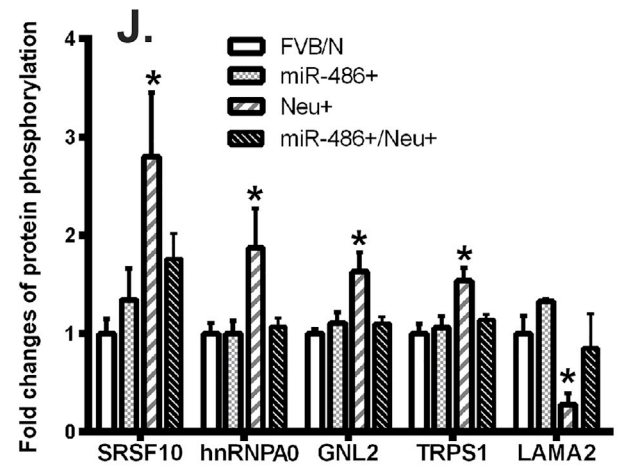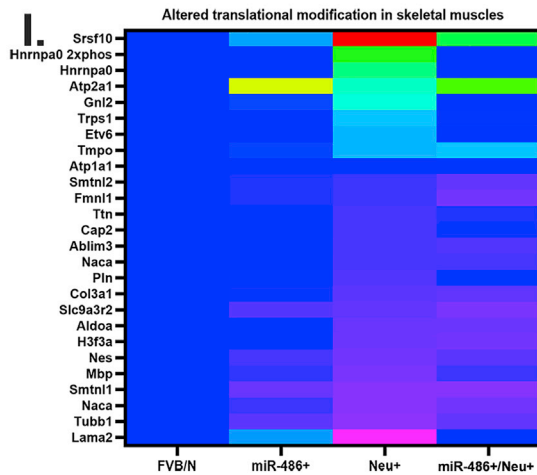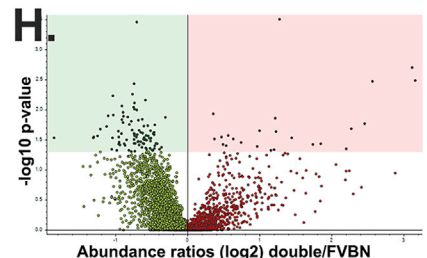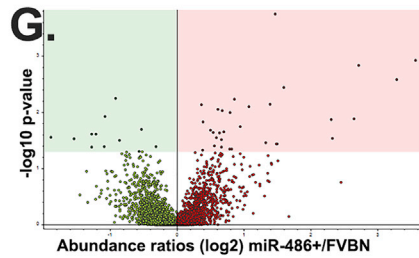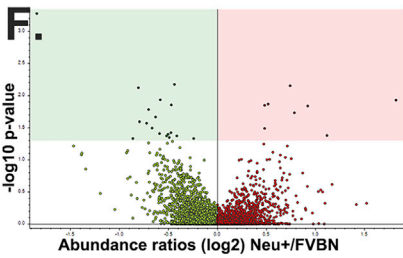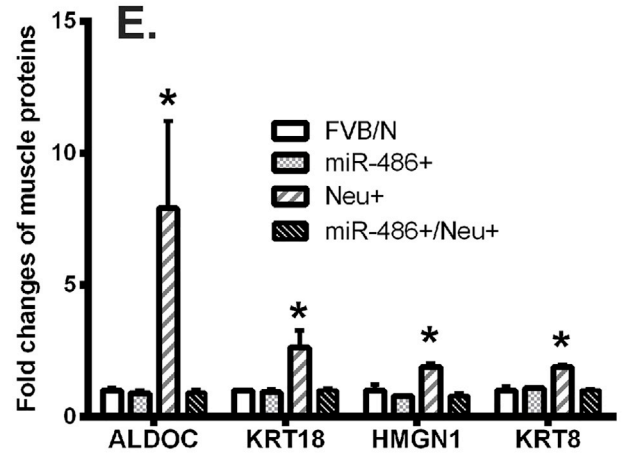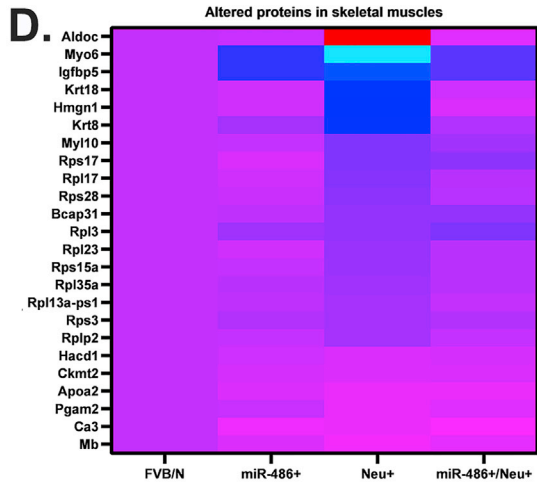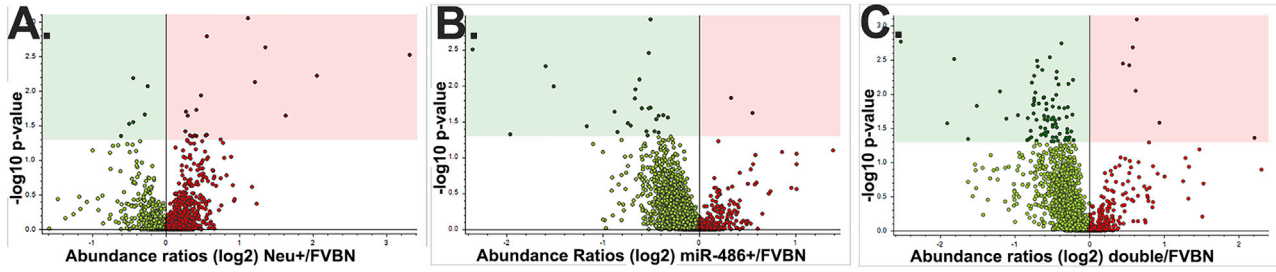
(legend on next page)

PIK3R1, which controls PIK3CA-dependent activation of AKT and whose loss of expression is associated with AKT activation,[33] is one of the targets of miR-486.

A previous study reported a Notch-Hey1-Mdm2 axis controlling the levels of p53 in skeletal muscle, and the Notch-p53 signaling axis plays an important role in skeletal muscle stem cell survival during activation, and this signaling axis declines with age.[34] We reported down-regulation of p53 in the skeletal muscle of Neu+ mice and suggested that Neu+ tumors accelerate skeletal muscle aging.[10] To examine relationship between miR-486 levels and p53 levels, we measured p53 levels in skeletal muscle of all four groups of mice. Reduced p53 levels in the skeletal muscle of Neu+ mice compared with control mice were observed (Figure 4D). Overexpression of miR-486 significantly reversed the tumor-induced loss of p53 in skeletal muscle, as p53 levels in the skeletal muscle of double-transgenic mice rebounded (Figure 4D). Interestingly, miR-486 overexpression in non-tumor-bearing mice did not alter skeletal muscle p53 levels, suggesting the existence of fine-tuned regulatory mechanism that controls p53 levels in skeletal muscle. Densitometric scanning results of all western blots are shown in Figure 4E.

The effects of tumor on skeletal muscle p53 are at transcriptional level as mRNA levels of *p53* were lower in skeletal muscle of Neu+ mice, which was partially reversed in double-transgenic mice (Figure 4F). It was previously reported that activation of Notch leads to upregulation of its downstream target *Hey1*, which increases p53 in skeletal muscle by repressing *Mdm2*.[10] *Hey1* mRNA levels were lower in skeletal muscle of Neu+ mice compared with control mice, and its levels were partially restored in double-transgenic mice (Figure 4F). However, we did not observe an effect of tumor or miR-486 overexpression on *Mdm2* levels. Thus, it is likely that although cancer causes deregulated Notch signaling, miR-486 is required for optimal Notch signaling in skeletal muscle to maintain p53 levels.

Global proteomics and phospho-proteomics reveal new targets of Neu+ tumors in skeletal muscle

To further reveal the effects of Neu+ tumors on skeletal muscle, which are reversible by miR-486, we isolated skeletal muscle myofibers from the fresh hindlimb muscles of mice from all four groups and performed global and phospho-proteomics. In global proteomics, 1,951 proteins and 14,566 peptide groups were identified. Among them, 1,791 master proteins were quantified (Table S1). Compared with FVB/N control group, levels of 18 proteins were elevated and six proteins were decreased in the skeletal muscle of Neu+ mice (Figure 5A). miR-486 overexpression in skeletal muscle resulted in increase of two proteins and the decrease of 25 proteins (Figure 5B). In double-transgenic mice compared with control mice, 81 proteins were decreased, and seven proteins were increased in myofibers (Figure 5C). Among 24 proteins that were altered in Neu+ mammary tumor-bearing mice compared with control mice, expression levels of 17 proteins were restored to levels detected in control mice upon miR-486 overexpression (Figure 5D). For example, Neu+ mammary tumors caused approximately eight-, three-, two-, and two-fold increases in fructose-bisphosphate aldolase C (ALDOC), keratin, type I cytoskeletal 18 (KRT18), non-histone chromosomal protein HMG-14 (HMGN1), and keratin, type II cytoskeletal 8 (KRT8), respectively, in skeletal muscle compared with control mice (Figure 5E). Co-overexpression of miR-486 with Neu+ *in vivo* reversed the Neu+ tumor-induced changes in these proteins.

In phospho-proteomics analysis, a total of 4,237 phosphopeptides were identified, and 3,869 were quantified (Table S2). Eight phosphopeptides were increased and 18 phosphopeptides were decreased in Neu+ tumor-bearing mice compared with FVB/N mice (Figure 5F). miR-486 overexpression in skeletal muscle itself caused increased levels of 31 phosphopeptides and decreased levels of 12 phosphopeptides compared with skeletal muscle of FVB/N mice (Figure 5G). In double-transgenic mice, 24 phosphopeptides were increased and 91 phosphopeptides were decreased (Figure 5H). These results suggest the effects of cancer- and muscle-specific overexpression of miR-486 on post-translational modifications of proteins in skeletal muscle. Among 26 significant changes caused by Neu+ mammary tumors, 16 phosphorylation activities were normalized (p > 0.5) upon overexpression of miR-486 (Figure 5I).

Proteins whose phosphorylation were altered in Neu+ tumor-bearing mice include heterogeneous nuclear ribonucleoprotein A0 (hnRNPA0), nucleolar GTP-binding protein 2 (GNL2), zinc finger transcription factor Trps1 (TRPS1), serine/arginine-rich splicing factor 10 (SRSF10), and laminin alpha 2 (LAMA2) (Figure 5J). Overexpression of miR-486 normalized phosphorylation of these proteins similar to that in FVB/N mice (Figure 5J). In Neu+ tumor-containing mice, increased hnRNPA0 phosphorylation occurred at serine 84, a known site for phosphorylation by the kinase MK2.[25] SRSF10 phosphorylation occurred at sites S199 and/or S201, which are known to

Figure 5. Global and phospho-proteomics analyses of skeletal muscle fibers of mice from four groups: FVB/N, miR-486+, Neu+ and miR-486+/Neu+ mice
Approximately 1 g fresh skeletal muscle tissue from the hindlimb from each group (n = 3) was collected at the end of behavioral tests with matched age (~28 weeks old) was analyzed. (A) Distribution of significantly altered proteins in the skeletal muscle fibers of Neu+ mice compared with FVB/N mice (n = 3 per group). (B) Distribution of significantly altered proteins in miR-486+ mice compared with FVB/N mice. (C) Distribution of significantly altered proteins in miR-486+/Neu+ mice compared with FVB/N mice (n = 3 per group). (D) Heatmap of significantly altered proteins in the skeletal muscle fibers of Neu+ mice (n = 3 per group), compared with proteins in FVB/N, miR-486+, and miR-486+/Neu+ mice. (E) Selected proteins that changed significantly in the Neu+ group but were normalized in miR-486+/Neu+ mice (p < 0.05; n = 3 per group). (F–H) Distribution of significantly altered phosphorylated proteins in the skeletal muscle fibers of Neu+ mice (n = 3 per group), miR-486+ mice (n = 3 per group), and miR-486+/Neu+ mice (n = 3 per group), respectively, compared with FVB/N group. (I) Heatmap of significantly altered phosphorylated proteins in Neu+ mice (n = 3 per group) compared with FVB/N, miR-486+, and miR-486+/Neu+ groups. (J) Selected phospho-proteins that changed significantly in Neu+ group but were normalized in miR-486+/Neu+ mice (p < 0.05; n = 3 per group). *Significance by comparison with FVB/N group.
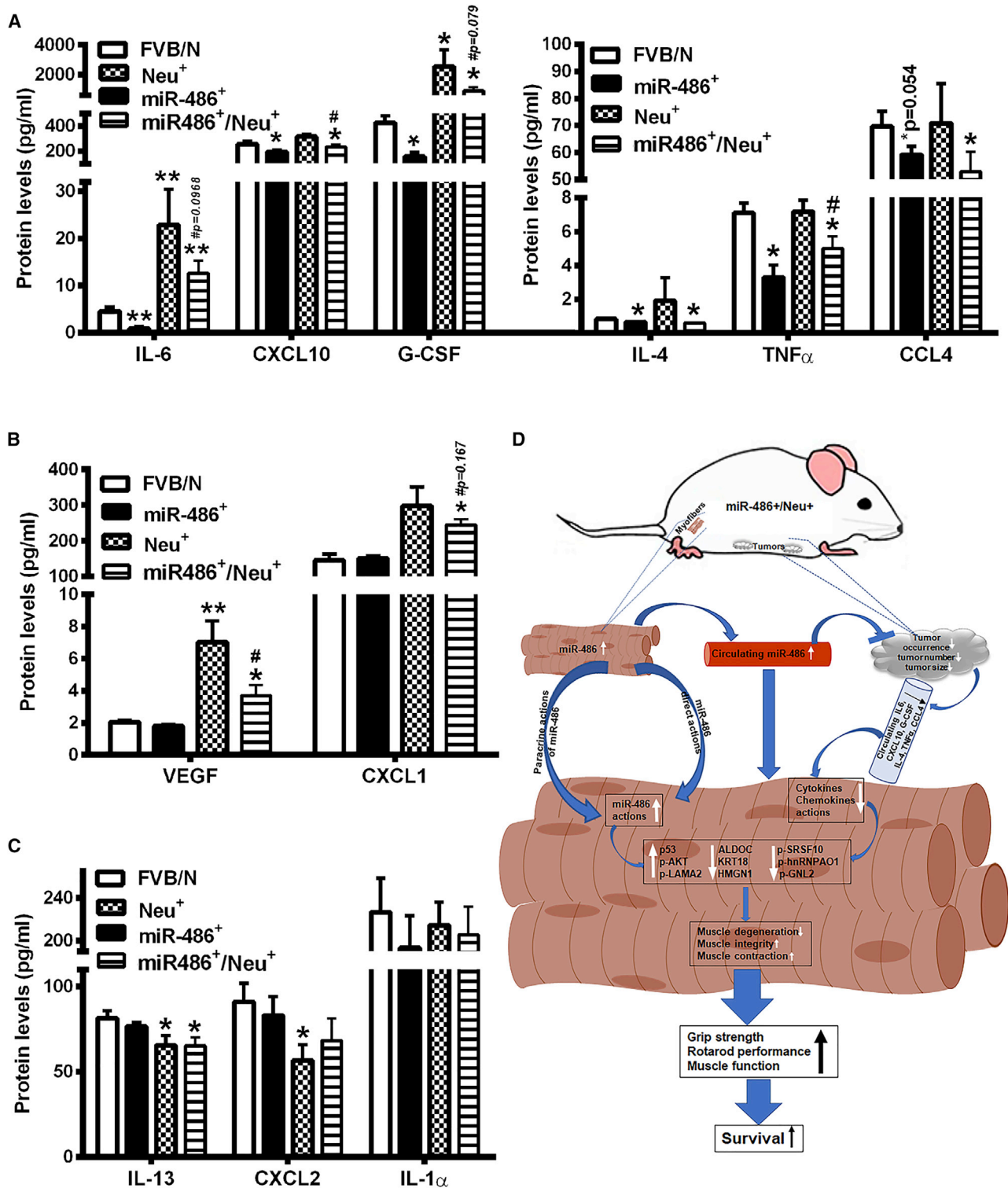
Figure 6. Skeletal muscle miR-486 regulates circulating cytokine/chemokines

(A) Skeletal muscle miR-486 reduced basal circulating levels of pro-inflammatory CCL4, CXCL10, G-CSF, IL-4, IL-6, and TNF-α. Mammary tumors increased the levels of several of these cytokines/chemokines in plasma, which were reversed in most cases upon miR-486 overexpression. (B) miR-486 reduced mammary tumor-induced up-regulation of VEGF in plasma. (C) miR-486 did not affect circulating levels of IL-13, CXCL2, and IL-1α. n = 9 per group (p < 0.05) for all cytokine analysis. *Significance by

(legend continued on next page)

be phosphorylated by a family of kinases called SR protein-specific kinases, and SRPK3 among them is expressed specifically in skeletal muscle.[23] These sites are also phosphorylated by CLK1-3.[24] Reduced phosphorylation of LAMA2 in Neu+ mice occurred at a consensus phosphorylation site for protein kinase A (RRQS).[35]

In order to reveal the interactions of altered proteins in the skeletal muscles noted above, we explored the network connections of proteins using the STRING protein-protein networks database.[36] We found that these proteins are functionally connected with one another either directly or indirectly (Figure S2). SRSF3 and SRSF10 directly interact with splicing protein SNRPD2 and nuclear ribonucleoprotein HNRNPA0, which is involved in post-transcriptional regulation of cytokine mRNAs.[37] These proteins also interact with multiple ribosomal proteins (i.e., RPLP2, RPS3, RPS17, and RPL23) involved in the translation of proteins associated with myogenesis, myofiber growth, and muscle contraction (i.e., TTN, DMD, MyoD, and PAX7), mainly via p53 and H3F3A (Figure S2). Additionally, proteins that regulate muscle energy (i.e., ALDOC, CKMT2, and ATP2A1) are involved in the network of skeletal muscle function. Therefore, Neu+ tumor-derived factors may affect the network of nuclear proteins (Figure S2, red oval), proteins that are involved in myogenesis, myofiber growth, and muscle contraction (Figure S2, blue circle), and proteins that are involved in muscle energy regulation (Figure S2, green circle).

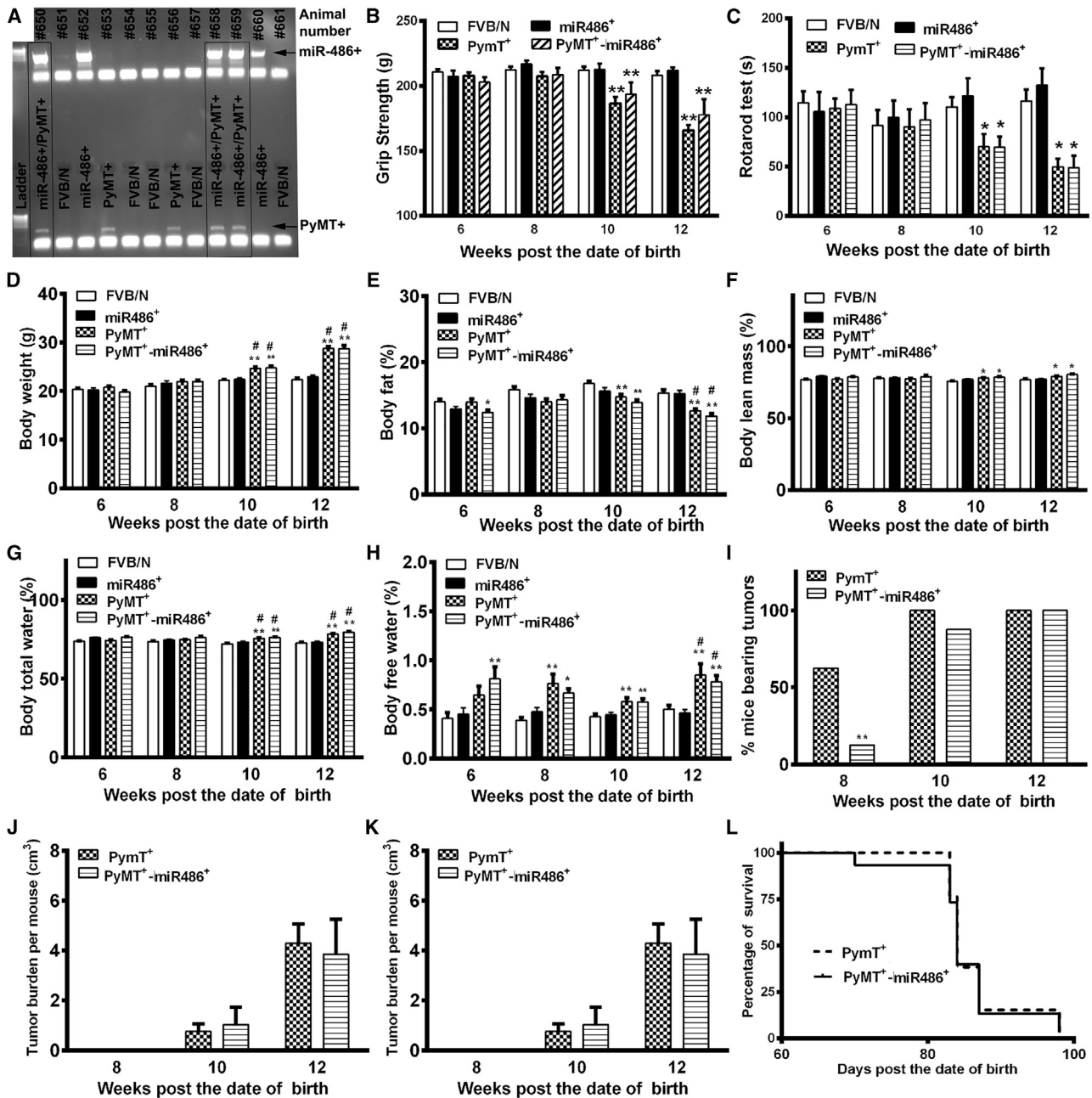### Skeletal muscle miR-486 has a systemic effect on circulating cytokines

We had previously reported that tumors cause changes of circulating cytokines/chemokines, and few of them can be normalized by treatment with NF-κB inhibitors.[9,10] To determine whether miR-486 can similarly normalize tumor-induced cytokines/chemokines, we measured plasma cytokines/chemokines in four group mice (Table S3). miR-486 displayed two distinct effects on plasma cytokines and chemokines. One effect was on overall cytokine/chemokine levels under healthy conditions and consequently reduction in their levels under tumor-bearing conditions. This effect appears to be dominant, as the levels of six cytokines/chemokines (CCL4, CXCL10, G-CSF, IL-4, IL-6, and TNF-α) were lower in miR-486 transgenic mice compared with control mice (Figure 6A). Levels of several of these cytokines were elevated in Neu+ transgenic mice compared with control mice, and double-transgenic mice displayed levels intermediate to those of Neu+ and control mice. The second effect was only on cytokines/chemokines that are aberrantly expressed in tumor-bearing mice. For example, mammary tumors resulted in the increase of VEGF in plasma but was normalized upon overexpression of miR-486 in skeletal muscles (Figure 6B). The effect of miR-486 on cytokines/chemokines showed some level of specificity, as the

levels of IL-13, CXCL2, and IL-1α were unaffected (Figure 6C). Thus, skeletal muscle miR-486 has an influence on systemic inflammation as well as tumor-induced changes in circulating factors (Figure 6D).

Specificity in the ability of miR-486 in limiting cancer-induced functional limitations

We had previously reported differences in cytokines and chemokines released by tumors on the basis of genomic aberrations.[7] For example, cell lines created from tumors in Neu+ and PyMT+ mice released distinct cytokines,[7] which may partly contribute to distinct differences in tumor latency and survival in two models (220 day survival in Neu+ versus 110 days in PyMT+). We also noted that lower skeletal muscle and circulating levels of miR-486 with accompanying functional limitations are consistent across both models, and pharmacologic inhibition of NF-κB overcomes functional limitation in both models. However, NF-κB inhibitor restored circulating and skeletal muscle levels of miR-486 only in the Neu+ model.[10] These observations promoted us to investigate whether the ability of miR-486 to restore skeletal muscle function is tumor type dependent. To address this possibility, we generated mice that are double-transgenic for PyMT and miR-486. The presence of both transgenes in double-transgenic miR-486+/PyMT+ mice was validated by genotyping (Figure 7A). Reductions of grip strength and rotarod performance were observed in PyMT+ mice with tumors, which is consistent with previous report,[9] but overexpression of miR-486 did not restore muscle function (Figures 7B and 7C). Unlike in Neu+ tumors, we observed an increase of miR-486 levels in tumors of miR-486+/PyMT+ mice compared with miR-486 levels in tumors of PyMT+ mice despite modest differences in tumor growth properties between two groups (Figure S1). We currently do not have an explanation as to why miR-486 levels in tumors of miR-486+/PyMT+ mice are higher compared with tumors in PyMT+ mice, but it could involve differences in tumor vasculature, as miR-486 is expressed in hematopoietic cells.[38] PyMT+ tumor associated weight gain (most likely due to tumor mass), body lean mass, body total and free water percentages, and body fat loss were unaffected by miR-486 (Figures 7D–7H). miR-486 overexpression, however, delayed tumor onset, as evident from lower tumor numbers in double-transgenic mice at 8 weeks of age compared with PyMT+ mice, but this delay is short-lived and ultimately did not have an effect on the number and volume of tumors or survival (Figures 7I–7L). These results imply that cancer-specific genomic aberrations and consequently degree of tumor aggressiveness influence the ability of skeletal muscle-derived miR-486 to affect tumor growth patterns and to overcome cancer-induced defects in skeletal muscle function. However, further investigation is needed to reveal the underlying mechanisms.

---

comparison with FVB/N group. #Significance by comparison with Neu+ group. (D) Schematic summary of the role of miR-486 in cancer-associated functional limitations. Skeletal muscle overexpression of miR-486 had direct and paracrine effects on skeletal muscles, resulting in changes in p-AKT, p53, and p-LAMA2 levels, leading to improvement of muscle integrity, muscle contraction, and functional performance such as grip strength and rotarod walking. Complementary to these effects on skeletal muscle, increased miR-486 through circulating system inhibited tumor occurrence and tumor growth, then reduced the impact of tumors on muscle function via downregulating circulating cytokines and chemokines.

Figure 7. miR-486 overexpression had limited effects on skeletal muscle phenotype of PyMT+ mice

(A) Confirmation of miR-486 and PyMT transgenes in mice. (B) Overexpression of miR-486 did not reverse PyMT+ tumor-induced reduction in grip strength (p < 0.005, control and miR-486+ versus PyMT+ and miR-486+/PyMT+; n = 12 per group). (C) Overexpression of miR-486 did not reverse PyMT+ tumor-induced reduction in rotarod performance (p < 0.005, control and miR-486+ versus PyMT+ and miR-486+/PyMT+; n = 12 per group). (D) Overexpression of miR-486 did not affect body weight in PyMT+ mice (n = 12 per group). (E) miR-486 did not affect body fat in PyMT+ mice (n = 12 per group). (F) miR-486 did not affect body lean mass in PyMT+ mice (n = 12). (G) miR-486 did not affect body total water in PyMT+ mice (n = 12/group). (H) miR-486 did not affect body free water in PyMT+ mice (n = 12/group). (I) miR-486 overexpression resulted in delayed development of tumors in PyMT+ mice (p < 0.005 at 8 weeks post-birth; n = 12 per group). (J and K) miR-486 did not ameliorate tumor burden in PyMT+ mice. (L) PyMT+ and miR-486+/PyMT+ mice displayed similar survival rates (n = 12 per group).

DISCUSSION

In this study, we demonstrate the role of miR-486 in attenuating cancer-induced skeletal muscle defects in a tumor subtype-dependent manner (Figure 6D). This study extends our previous observations that established biomarker potential of miR-486 in identifying breast cancer-induced functional limitations. This report further demonstrates functional consequences of reduced skeletal muscle miR-486 expression and the ability of miR-486 overexpressed in skeletal muscle to overcome cancer-induced functional limitation in at least one breast cancer subtype. Approximately 20% of breast cancers are HER2 positive, and in a model representing this breast cancer subtype, miR-486 was able to reduce cancer-induced functional limitations.[10] Elevating skeletal muscle miR-486 itself was able to reduce aggressiveness of mammary tumor, suggesting that myokines or miR-486 secreted by skeletal muscle or the paracrine effects of skeletal muscle miR-486 on systemic inflammation can exert anti-tumor activity (Figure 6D). In this regard, irisin is a skeletal muscle-derived factor induced upon exercise with anti-tumor activity,[29] and its circulating levels are lower in breast cancer patients compared with healthy controls.[39] A recent study has identified musclin (also called osteocrin), a myokine, as a skeletal muscle-derived factor that prevents cardiac fibrosis and heart failure.[40] Musclin also has anti-inflammatory properties.[41] It is possible that miR-486-mediated restoration of muscle function enhances production and release of these myokines from the skeletal muscle. However, new model systems, such as inducible expression of miR-486 in skeletal muscle, need to be developed to delineate whether tumor-suppressor function of miR-486 is responsible for improved skeletal muscle function or miR-486-mediated improvement in skeletal muscle function is responsible for reduced tumor growth in double-transgenic mice.

The biological role of miR-486 has been studied extensively, as its expression is lower in skeletal muscle of DMD patients and its skeletal muscle-specific overexpression in skeletal muscle could overcome muscular defects in DMD models.[16,17] As miR-486 was able to rescue the skeletal muscle defects in Neu+ tumors, at the molecular level, there could be some similarity in skeletal muscle defects in Neu+ tumors and various forms of muscular dystrophy. Results of global and phospho-proteomics analyses suggest such a possibility. For example, we observed elevated phosphorylation of hRNAPA0 at S84, which is typically phosphorylated by MK2. MK2 is activated downstream of p38 kinase, and elevated MK2 activity in skeletal muscle is observed in DMD models.[42] We observed lower levels of LAMA2 phosphorylation at a PKA consensus site in the skeletal muscle of Neu+ mice. Lower PKA activity is observed in dystrophic skeletal muscle.[43] However, at present, it is unclear whether phosphorylation at this site is required for LAMA2 function and reduced phosphorylation diminishes its function. LAMA2 is a cell surface-anchored protein that is connected to cytoplasmic dystrophin through dystroglycans to generate dystrophin-associated glycoprotein complex.[44] Mutational inactivation of this protein is associated with a spectrum of muscular dystrophy ranging from severe congenital muscular dystrophy type 1A to less severe later onset dystrophy, which is largely due to death of immature myofibers.[45]

Neu+ tumor-mediated changes in SRSF10 and hRNAPA0 phosphorylation clearly indicate the effects of tumor on mRNA splicing and mRNA stability in skeletal muscle. MK2 phosphorylated hnRNPA0 stabilizes GADD45α, which mediates skeletal muscle atrophy.[46] GADD45α levels are elevated during the early phase of DMD.[47] Thus, elevated activated hRNPA0 in skeletal muscle of Neu+ mice could promote muscle atrophy through GADD45α, which needs further investigation. It has been reported that SRSF10 is critical for myoblast differentiation and glucose production via the PGC1α pathway.[48] SRSF10 is phosphorylated by both the SRPK family and CLK family of kinases, and CLK1 inhibitors have been suggested as potential therapy for DMD[49]. Alternative splicing is the major mechanism of proteome diversification in skeletal muscle,[23] and cancer-induced factors could influence this process by elevating the activity of SRSF10. Phosphorylated SRSF10 is an activator of alternative splicing, and its targets in skeletal muscle include the transcription factors *Mef2A*, *FMR1 autosomal homolog 1*, *leucine-rich repeat interacting protein 1*, and *F-actin capping protein subunit beta*.[23] Mef2A undergoes extensive alternative splicing in myotonic dystrophy.[50] Thus, there appears to be substantial parallel between skeletal muscle defects observed under Neu+ tumor conditions and various muscular dystrophies.

Metabolic pathway alterations in cachectic skeletal muscle have been reported previously,[51] and a recent study demonstrated the effects of miR-486 knockout on metabolic pathway.[18] Thus, cancer-induced metabolic pathway alterations in skeletal muscle could be due partly to reduced levels of miR-486. Consistent with this possibility, skeletal muscle of Neu+ mice contained higher levels of ALDOC, and this increase was attenuated upon miR-486 replenishment.[18] ALDOC is involved in the carbohydrate catabolic process that contribute to the generation of small amounts of ATP (energy) and NADH (reducing power), and gluconeogenesis.[52] Alterations in carbohydrate metabolism have been reported in canine models of DMD[53] and in cancer cachexia.[54] Whether ALDOC plays a functional role in cancer-induced skeletal muscle dysfunction needs further investigation. In addition, we observed an effect of miR-486 on body fat. Although Neu+ animals with tumors displayed lower body fat compared with control animals, this body fat loss was delayed in double-transgenic mice. Elevated circulating miR-486 levels were found in children with obesity[55,56] and patients with metabolic syndrome.[57] These changes in circulating miR-486 levels are significantly associated with the percentage of body fat mass and clinical measures related to obesity.[58] High glucose increases miR-486 expression that regulates adipogenic differentiation in human adipose tissue-derived mesenchymal stem cells.[59] Additionally, miR-486 can inhibit the transcription factors such as FOXO1,[60] which play a role in insulin resistance and triglyceride metabolism.[61] Therefore, miR-486 might be directly or indirectly involved in energy metabolism, which is consistent with observations in miR-486-knockout mice.[18]

We also observed an effect of Neu+ tumors on HMG-14 expression in skeletal muscle, which was mitigated upon miR-486 overexpression. HMG-14/HMGN1 is a high mobility group nucleosome binding

protein, and its expression is downregulated during myogenesis. However, its functional role in myogenesis remains controversial.[62] It is also unknown whether upregulation of this protein in skeletal muscle in cancer has an impact on functional limitations or cachexia. Further studies are needed to determine the impact of this gene in cancer cachexia.

The effect of skeletal muscle expression of miR-486 on systemic cytokines/chemokine levels is one of surprising observations of this study. How miR-486 effects these specific cytokines or the cell types in which miR-486 alters their expression is unknown. As per miRDB database, miR-486 targets multiple transcription factors and chromatin modifiers such as FOXO1, ZNF331, MRTFA, ARID4B, and HAT1 and few of these transcription regulators could control the expression of these cytokines/chemokines. miR-486 less likely effects cytokine/chemokine production by the tumor microenvironment as miR-486 levels in tumors of Neu+, PyMT+, miR-486+/Neu+, and miR-486+/PyMT+ mice did not show consistent pattern (Figure S1). Moreover, IL-6 levels in miR-486+ mice without any tumors were lower compared with control mice, suggesting that a tumor-independent systemic effect of skeletal muscle miR-486 is responsible for differences in levels of at least few of the circulating cytokines/chemokines. Whatever the mechanisms involved, the ability of miR-486 to reduce specific cytokines/chemokines should have an impact on skeletal muscle biology. Elevated IL-6 in plasma causes skeletal muscle atrophy via STAT3/5 pathways, and IL-6 receptor inhibition suppresses muscle MuRF1 expression and attenuates muscle atrophy.[63] Circulating IL-6 levels are also elevated in DMD patients, and anti-IL-6 therapies are suggested in these patients.[64] Similar to Neu+ model, CXCL10 levels are elevated in serum of DMD patients.[65] CXCL10 is an essential inflammatory mediator, which together with other cytokines such as IL-6, causes chronic myopathies in cancer conditions.[66] Although its primary clinical application is for immunodeficiency, particularly in neutropenia, G-CSF has recently gained more attention for its role in myopathies. Elevated circulating G-CSF levels were reported in *mdx* mice,[67] similar to our observation in Neu+ tumor-bearing mice. In IL-6-null mice, macrophages produce less G-CSF,[68] indicating the integrations of IL-6 and G-CSF signaling during the disease conditions of cancer, similar to DMD.

In summary, this study provides compelling evidence for the role of miR-486 in reversing skeletal defects observed in certain cancer types (Figure 6D). As miR-486 expression did not affect skeletal muscle defects in a PyMT+ model, cancer genome and consequently aggressiveness of the disease have a direct influence on the type and severity of skeletal muscle defect and the ability of miR-486 to overcome these defects. Better understanding and therapeutic targeting of cancer-induced skeletal muscle defects, therefore, requires integration of cancer genomics with skeletal muscle biology.

MATERIALS AND METHODS
Animals and functional tests
Animal protocols were approved by the Institutional Animal Care and Use Committee at the Indiana University School of Medicine and were in accordance with guidelines from the National Institutes of Health regarding the use and care of experimental animals. Male MCK-miR-486+ mice (hereafter miR-486+ mice) in the C57BL/6 background have been described previously[17] and then backcrossed into FVB/N background for six generations (Figure 1). Male Neu+ and PyMT+ mice on FVB/N background were purchased from Jackson Laboratory. To generate double-transgenic mice, female miR-486+ mice were crossed with male PyMT+ or Neu+ mice. Only female mice were used for further evaluation of tumor progression (tumor onset time, size, and volume), body composition alteration (body weight, body fat, lean mass, body free water, and total water), and functional limitation studies (grip strength, rotarod performance in live animals, and *ex vivo* muscle contraction studies).

Body composition, behavioral tests, and tumor reading were performed as described in our previous studies.[9,10] Briefly, the quantification of body fat, lean mass, body free water, and total water was performed using small-animal EchoMRI-100 (EchoMRI, Houston, TX). Animals were physically restrained in a test tube when measurements were taken, and all measurements were normalized to the percentage of mouse body weight. To evaluate whole-body strength in mice, the absolute grip strength (peak force expressed in gram force) was recorded by means of a grip strength meter (Bioseb In Vivo Instruments, Pinellas Park, FL) by placing mice on a wire mesh connected to a test meter, pulling the tail directly back parallel to the mesh surface, and then recording the amount of force. Three trials of each test were performed with minimum 5 min intervals, and the average value from the three recordings was presented. In the case of Neu+ mice, body composition and grip strength were measured at 4 week intervals starting at 16 weeks post-birth, before mammary tumor occurrence. However, in the case of PyMT+ mice, tests were performed at 2 week intervals starting at 6 weeks post-birth. Rotarod performance (Harvard Apparatus) was measured to evaluate muscle function and muscle fatigue at the end of the experiment. The time a mouse was able to stay on a rotating rod at 10 rpm was recorded three times at minimum 5 min intervals, and the average from the three recordings was presented. The cut-off time was 3 min. Mammary tumor number per mouse and tumor size were monitored periodically, and tumor volume was calculated as (length) $\times$ (width)^2/2.

Blood and tissues were collected at the time of sacrifice for miRNA, mRNA, and protein preparation or for histological analysis. Time of sacrifice in survival test was based on recommendation of euthanasia by the attending veterinarian. Statistical analysis was performed by one-way ANOVA or nonparametric t test using GraphPad Prism at each time point, and data are presented as mean ± SEM. A p value of ≤ 0.05 was considered to indicate statistical significance.

Ex vivo skeletal muscle-specific force measurements
Skeletal muscle contraction force studies using intact extensor digitorum longus muscles from four groups of mice were performed as described previously,[10] as the EDL is commonly studied during cancer-induced muscle dysfunction, particularly in affected glycolytic muscles.[69,70] Briefly, at the end of experiment (~28-week-old

mice), intact isolated extensor digitorum longus muscles from four groups of mice were attached to an isometric force transducer (model 407A; Aurora Scientific) between platinum stimulating electrodes in a glass chamber containing modified Tyrode solution. A force-frequency relationship was determined by measuring muscle contraction force at a range of frequencies (1–200 Hz; model 701C; Aurora Scientific) to obtain a maximum tetanic force plateau. An endurance protocol to measure fatigue was run by inducing a tetanic response (70 Hz, 300 ms) and repeating for 50 cycles (EDL). Stimulation was controlled by Dynamic Muscle Control software and analyzed using Dynamic Muscle Analysis software (dmc version 5.300, dma version 5.010; Aurora Scientific). The specific force (millinewtons) was calculated at various stimulating points from individual EDL muscle and averaged by group.

RNA extraction and quantitative reverse transcription PCR

Mouse blood was collected at the time of sacrifice in a K2 EDTA-coated tube, then centrifuged at 2,000 rpm for 15 min at 4°C, and supernatant was transferred into a clean Eppendorf tube for storage at −80°C. A Qiagen miRNeasy serum/plasma kit (#217184; Qiagen) was used to isolate miRNA from 200 μL stored plasma. Tibialis anterior (TA) and gastrocnemius muscles from the hindlimb of the mouse were harvested, snap-frozen, and stored at −80°C. A Qiagen miRNeasy Mini Kit (#217004) or Qiagen RNeasy Mini Kit (#74106) was used to isolate miRNA or total RNA from ~30 mg of stored muscle following the manufacturer's instructions.

Five microliters of miRNAs extracted from plasma (20 ng/μL) were used for cDNA synthesis using a Taqman miRNA Reverse Transcription Kit (Applied Biosystems). Total RNA from muscle tissues (200 ng) was reverse transcribed into cDNAs using the Bio-Rad iScript cDNA synthesis kit in a final volume of 20 μL. Quantitative PCR (qPCR) was performed using Taqman universal PCR mix (Applied Biosystems) and specific primers. miRNA primers for U6 (#001973), miR-486 (#001278), and miR-202 (#002579) and mRNA primers for HSP90ab (#Mm00833431-g1), p53 (#Mm01354484-m1), Mdm2 (#Mm01233138_m1), and Hey1 (#Mm00468865_m1) were purchased from Applied Biosystems. Each amplification reaction was performed in duplicate in a final volume of 20 μL with 4 μL cDNA. The expression levels of miR-486 were normalized to miR-202 (mouse plasma) and U6 (skeletal muscle) using the $2-\Delta\Delta Ct$ method, as described in a previous study.[7] The expression levels of mRNAs were normalized to HSP90ab.

Western blotting

We used tibialis anterior muscle to determine cancer-induced signaling pathway alterations in skeletal muscle, as changes in TA muscle function are frequently observed in models of cancer cachexia.[71] TA muscle (~30 mg fresh tissue) was lysed in RIPA buffer with protease/phosphatase inhibitors (catalog no. 5872S; Cell Signaling Technology) and then homogenized using Qiagen Tissue Lyser LT with metal beads at a speed of 50 Hz for 3 min, followed by 10 s of sonication. Thirty micrograms of proteins in 25 μL volume were used for western blotting, as described previously.[10] Primary an-

tibodies against AKT (catalog no. 4691, rabbit; Cell Signaling Technology), p-AKT (S473; catalog no. 4060, rabbit; Cell Signaling Technology), PTEN (catalog no. 9188, rabbit; Cell Signaling Technology) and p53 (catalog no. 32532, rabbit; Cell Signaling Technology) were used for western blots. Anti-rabbit IgG conjugated with horseradish peroxidase (HRP) (catalog no. 7074S; Cell Signaling Technology) was used as a secondary antibody, and the blot was developed using the substrate solution as per the manufacturer's instructions (catalog no. 32106; Thermo Fisher Scientific). Autoradiograms were scanned and quantified by using NIH ImageJ software. Protein levels were normalized to total proteins in lysates by Ponceau S staining.[10] Figure S3 provides copies of original unprocessed western blots of all figures.

Histology and immunohistochemistry

TA and gastrocnemius muscles were fixed with 10% buffer formalin and stored in a cold room. For H&E staining, formalin-fixed tissues were paraffin-embedded, sliced, stained in the pathology lab, and analyzed by a pathologist. For immunofluorescence, formalin-fixed tissues were transferred to 20% sucrose in PBS for 24 h, sliced with cryostat at 10 μm, mounted on positively charged slides, then washed with PBS three times and incubated with COX-IV antibody (1:1,000; #ab16056; Abcam). The next day, sections were washed three times with PBS and subsequently incubated with goat anti-rabbit IgG (H&L) and Alexa Fluor 488 (catalog no. 32731; Invitrogen) secondary antibody for 1 h at room temperature. After a final wash with PBS, sections were sealed by mounting media with DAPI and viewed and imaged under a Keyence BZ-X800 fluorescent microscope (Keyence, Farmington Hills, MI). For ECM histochemical examination, formalin-fixed, frozen sliced sections were washed with PBS three times and then incubated with Texas red-conjugated wheat germ agglutinin (WGA; 1:1,000; #W21405; Invitrogen) for 1 h at room temperature, followed by wash with PBS three times, then viewed and imaged with a Keyence BZ-X800 fluorescent microscope. COX-IV and WGA staining was quantified by measuring labeled area using NIH ImageJ software. The area occupied by staining was expressed relative to the total area of the muscle cross section.

Analysis of global proteins and post-translational modifications

Approximately 1 g fresh skeletal muscle tissues was dissected from the hindlimb of each mouse at the end of behavioral tests with matched age (~28 weeks old) and digested with mouse muscle dissociation kit (#130-098-305; MASC) for 30 min at 37°C in water bath, then dissociated with C tube (#130-093-237; MASC) using m_muscle_01_01 program set in GentleMACS Dissociator (#130-093-235). After another 30 min incubation in 37°C water bath with shaking every 5 min, digested tissue was diluted with DMEM medium and centrifuged at 200 rpm for 30 s. Top supernatant was transferred to a Petri dish, and large fiber debris was removed under light microscope. Next, supernatant underwent a series of steps, including washing and blood cell lysis, as described in the mouse muscle dissociation kit (#130-098-305; MASC). Following final centrifuge, the top supernatant was discarded, and the myofiber pellets were saved for the analysis of global

proteins and post-translational modifications. In brief, samples were lysed in 8 M urea and 50 mM Tris (pH 8.5). Following reduction in 5 mM TCEP, alkylation with 10 mM CAM, protein digestion with trypsin/LysC, 25 μg from each sample was used for global analysis, and 3,000 μg protein from each sample was used for phosphopeptide enrichment. Global and enriched phosphopeptides were separately TMT-labeled (TMTpro lot VJ316536) and offline high-pH fractionated. Finally, samples were run on Eclipse Orbitrap mass spectrometer with FAIMS pro (Thermo Fisher Scientific) and searched against reviewed and unreviewed *Mus musculus* UniProt database plus common contaminants on PD 2.5 (additional details in Supplemental methods). Proteome data are deposited with ProteomeXchange Consortium (project accession number PXD028554).

Plasma cytokine profiling
Circulating cytokines and chemokines were profiled and analyzed as described previously.[9,10] Briefly, circulating cytokines were measured using 100 μL plasma and a MILLIPLEX MAP Mouse Cytokine/Chemokine Magnetic Bead Panel (MCYTMAG-70K-PX32; Millipore) that measures 32 cytokines/chemokines from limited samples. TGF-β1, TGF-β2, and TGF-β3 were measured separately. Each group contained plasma samples from nine animals. Those samples with no detectable values were given a score of zero for the analyses.

Statistical analysis
Data were analyzed using two-factor (miR-486+ and Neu+) analysis of variance or one-way ANOVA with Tukey's multiple-comparisons test for comparisons between multiple groups with GraphPad Prism version 9 software (GraphPad, San Diego, CA). Unpaired parametric t tests were used for comparisons between two groups. A p value of <0.05 was considered to indicate statistical significance.

SUPPLEMENTAL INFORMATION
Supplemental information can be found online at https://doi.org/10.1016/j.omtn.2022.03.009.

ACKNOWLEDGMENT

AUTHOR CONTRIBUTIONS

DECLARATION OF INTERESTS

REFERENCES
1. Jiang, M., Li, X., Quan, X., Yang, X., Zheng, C., Hao, X., Qu, R., and Zhou, B. (2018). MiR-486 as an effective biomarker in cancer diagnosis and prognosis: a systematic review and meta-analysis. Oncotarget *9*, 13948–13958. https://doi.org/10.18632/oncotarget.24189.

2. Li, C., Zheng, X., Li, W., Bai, F., Lyu, J., and Meng, Q.H. (2018). Serum miR-486-5p as a diagnostic marker in cervical cancer: with investigation of potential mechanisms. BMC Cancer *18*, 61. https://doi.org/10.1186/s12885-017-3753-z.

3. Tanaka, M., Oikawa, K., Takanashi, M., Kudo, M., Ohyashiki, J., Ohyashiki, K., and Kuroda, M. (2009). Down-regulation of miR-92 in human plasma is a novel marker for acute leukemia patients. PLoS one *4*, e5532. https://doi.org/10.1371/journal.pone.0005532.

4. Resnick, K.E., Alder, H., Hagan, J.P., Richardson, D.L., Croce, C.M., and Cohn, D.E. (2009). The detection of differentially expressed microRNAs from the serum of ovarian cancer patients using a novel real-time PCR platform. Gynecol. Oncol. *112*, 55–59. S0090-8258(08)00683-5 [pii]. https://doi.org/10.1016/j.ygyno.2008.08.036.

5. Chen, X., Ba, Y., Ma, L., Cai, X., Yin, Y., Wang, K., Guo, J., Zhang, Y., Chen, J., Guo, X., et al. (2008). Characterization of microRNAs in serum: a novel class of biomarkers for diagnosis of cancer and other diseases. Cell Res. *18*, 997–1006, cr2008282 [pii] 10.1038/cr.2008.282.

6. Boeri, M., Verri, C., Conte, D., Roz, L., Modena, P., Facchinetti, F., Calabro, E., Croce, C.M., Pastorino, U., and Sozzi, G. (2011). MicroRNA signatures in tissues and plasma predict development and prognosis of computed tomography detected lung cancer. Proc. Natl. Acad. Sci. U S A *108*, 3713–3718. https://doi.org/10.1073/pnas.1100048108.

7. Chen, D., Goswami, C.P., Burnett, R.M., Anjanappa, M., Bhat-Nakshatri, P., Muller, W., and Nakshatri, H. (2014). Cancer affects microRNA expression, release, and function in cardiac and skeletal muscle. Cancer Res. *74*, 4270–4281. https://doi.org/10.1158/0008-5472.CAN-13-2817.

8. Rask, L., Balslev, E., Sokilde, R., Hogdall, E., Flyger, H., Eriksen, J., and Litman, T. (2014). Differential expression of miR-139, miR-486 and miR-21 in breast cancer patients sub-classified according to lymph node status. Cell Oncol. (Dordr). *37*, 215–227. https://doi.org/10.1007/s13402-014-0176-6.

9. Wang, R., Bhat-Nakshatri, P., Padua, M.B., Prasad, M.S., Anjanappa, M., Jacobson, M., Finnearty, C., Sefcsik, V., McElyea, K., Redmond, R., et al. (2017). Pharmacological dual inhibition of tumor and tumor-induced functional limitations in a transgenic model of breast cancer. Mol. Cancer Ther. *16*, 2747–2758. https://doi.org/10.1158/1535-7163.MCT-17-0717.

10. Wang, R., Kumar, B., Bhat-Nakshatri, P., Prasad, M.S., Jacobsen, M.H., Ovalle, G., Maguire, C., Sandusky, G., Trivedi, T., Mohammad, K.S., et al. (2021). Aging-associated skeletal muscle defects in HER2/Neu transgenic mammary tumor model. JCSM Rapid Commun. 4, 24–39. https://doi.org/10.1002/rco2.23.

11. Wang, R., Bhat-Nakshatri, P., Zhong, X., Zimmers, T., and Nakshatri, H. (2021). Hormonally regulated myogenic miR-486 influences sex-specific differences in cancer-induced skeletal muscle defects. Endocrinology. https://doi.org/10.1210/endocr/bqab142.

12. Buckingham, M., and Rigby, P.W. (2014). Gene regulatory networks and transcriptional mechanisms that control myogenesis. Dev. Cell 28, 225–238. https://doi.org/10.1016/j.devcel.2013.12.020.

13. Song, L., Lin, C., Gong, H., Wang, C., Liu, L., Wu, J., Tao, S., Hu, B., Cheng, S.Y., Li, M., and Li, J. (2013). miR-486 sustains NF-kappaB activity by disrupting multiple NF-kappaB-negative feedback loops. Cell Res 23, 274–289. https://doi.org/10.1038/cr.2012.174.

14. Hitachi, K., Nakatani, M., and Tsuchida, K. (2014). Myostatin signaling regulates Akt activity via the regulation of miR-486 expression. Int. J. Biochem. Cel. Biol. 47, 93–103. https://doi.org/10.1016/j.biocel.2013.12.003.

15. Small, E.M., O'Rourke, J.R., Moresi, V., Sutherland, L.B., McAnally, J., Gerard, R.D., Richardson, J.A., and Olson, E.N. (2010). Regulation of PI3-kinase/Akt signaling by muscle-enriched microRNA-486. Proc. Natl. Acad. Sci. U S A 107, 4218–4223. https://doi.org/10.1073/pnas.1000300107.

16. Alexander, M.S., Casar, J.C., Motohashi, N., Vieira, N.M., Eisenberg, I., Marshall, J.L., Gasperini, M.J., Lek, A., Myers, J.A., Estrella, E.A., et al. (2014). MicroRNA-486-dependent modulation of DOCK3/PTEN/AKT signaling pathways improves muscular dystrophy-associated symptoms. J. Clin. Invest. 124, 2651–2667. https://doi.org/10.1172/JCI73579.

17. Alexander, M.S., Casar, J.C., Motohashi, N., Myers, J.A., Eisenberg, I., Gonzalez, R.T., Estrella, E.A., Kang, P.B., Kawahara, G., and Kunkel, L.M. (2011). Regulation of DMD pathology by an ankyrin-encoded miRNA. Skeletal Muscle 1, 27. https://doi.org/10.1186/2044-5040-1-27.

18. Hightower, R., Samani, A., Reid, A., English, K., Lopez, M., Doyle, J., Conklin, M., Schneider, D., Bamman, M., Widrick, J., et al. (2021). miR-486 is an epigenetic modulator of Duchenne muscular dystrophy pathologies. Preprint at bioRxiv. https://doi.org/10.1101/2021.06.14.448387.

19. Summermatter, S., Bouzan, A., Pierrel, E., Melly, S., Stauffer, D., Gutzwiller, S., Nolin, E., Dornelas, C., Fryer, C., Leighton-Davies, J., et al. (2017). Blockade of metallothioneins 1 and 2 increases skeletal muscle mass and strength. Mol. Cell Biol. 37. https://doi.org/10.1128/MCB.00305-16.

20. Braithwaite, D., Satariano, W.A., Sternfeld, B., Hiatt, R.A., Ganz, P.A., Kerlikowske, K., Moore, D.H., Slattery, M.L., Tammemagi, M., Castillo, A., et al. (2010). Long-term prognostic role of functional limitations among women with breast cancer. J. Natl. Cancer Inst. 102, 1468–1477. https://doi.org/10.1093/jnci/djq344.

21. Baracos, V.E., Martin, L., Korc, M., Guttridge, D.C., and Fearon, K.C.H. (2018). Cancer-associated cachexia. Nat. Rev. Dis. Primers 4, 17105. https://doi.org/10.1038/nrdp.2017.105.

22. Shachar, S.S., Deal, A.M., Weinberg, M., Nyrop, K.A., Williams, G.R., Nishijima, T.F., Benbow, J.M., and Muss, H.B. (2017). Skeletal muscle measures as predictors of toxicity, hospitalization, and survival in patients with metastatic breast cancer receiving taxane-based chemotherapy. Clin. Cancer Res. 23, 658–665. https://doi.org/10.1158/1078-0432.CCR-16-0940.

23. Nakka, K., Ghigna, C., Gabellini, D., and Dilworth, F.J. (2018). Diversification of the muscle proteome through alternative splicing. Skeletal muscle 8, 8. https://doi.org/10.1186/s13395-018-0152-3.

24. Keshwani, M.M., Aubol, B.E., Fattet, L., Ma, C.T., Qiu, J., Jennings, P.A., Fu, X-D., and Adams, J.A. (2015). Conserved proline-directed phosphorylation regulates SR protein conformation and splicing function. Biochem. J. 466, 311–322. https://doi.org/10.1042/BJ20141373.

25. Reinhardt, H.C., Hasskamp, P., Schmedding, I., Morandell, S., van Vugt, M.A., Wang, X., Linding, R., Ong, S.E., Weaver, D., Carr, S.A., and Yaffe, M.B. (2010). DNA damage activates a spatially distinct late cytoplasmic cell-cycle checkpoint network controlled by MK2-mediated RNA stabilization. Mol. Cell 40, 34–49. https://doi.org/10.1016/j.molcel.2010.09.018.

26. Kim, H., Kim, M.C., and Asada, H.H. (2019). Extracellular matrix remodelling induced by alternating electrical and mechanical stimulations increases the contraction of engineered skeletal muscle tissues. Sci. Rep. 9, 2732. https://doi.org/10.1038/s41598-019-39522-6.

27. Wang, R., and Nakshatri, H. (2020). Systemic actions of breast cancer facilitate functional limitations. Cancers (Basel) 12. https://doi.org/10.3390/cancers12010194.

28. Darkwah, S., Park, E.J., Myint, P.K., Ito, A., Appiah, M.G., Obeng, G., Kawamoto, E., and Shimaoka, M. (2021). Potential roles of muscle-derived extracellular vesicles in remodeling cellular microenvironment: proposed implications of the exercise-induced myokine, irisin. Front. Cell Dev. Biol. 9, 634853. https://doi.org/10.3389/fcell.2021.634853.

29. Maalouf, G.E., and El Khoury, D. (2019). Exercise-induced irisin, the fat browning myokine, as a potential anticancer agent. J. Obes. 6561726. https://doi.org/10.1155/2019/6561726.

30. Wang, J., Tian, X., Han, R., Zhang, X., Wang, X., Shen, H., Xue, L., Liu, Y., Yan, X., Shen, J., et al. (2014). Downregulation of miR-486-5p contributes to tumor progression and metastasis by targeting protumorigenic ARHGAP5 in lung cancer. Oncogene 33, 1181–1189. https://doi.org/10.1038/onc.2013.42.

31. Yu, S., Geng, S., and Hu, Y. (2018). miR-486-5p inhibits cell proliferation and invasion through repressing GAB2 in non-small cell lung cancer. Oncol. Lett. 16, 3525–3530. https://doi.org/10.3892/ol.2018.9053.

32. Chen, Y., and Wang, X. (2020). miRDB: an online database for prediction of functional microRNA targets. Nucleic Acids Res. 48, D127–D131. https://doi.org/10.1093/nar/gkz757.

33. Li, X., Mak, V.C.Y., Zhou, Y., Wang, C., Wong, E.S.Y., Sharma, R., Lu, Y., Cheung, A.N.Y., Mills, G.B., and Cheung, L.W.T. (2019). Deregulated Gab2 phosphorylation mediates aberrant AKT and STAT3 signaling upon PIK3R1 loss in ovarian cancer. Nat. Commun. 10, 716. https://doi.org/10.1038/s41467-019-08574-7.

34. Liu, L., Charville, G.W., Cheung, T.H., Yoo, B., Santos, P.J., Schroeder, M., and Rando, T.A. (2018). Impaired Notch signaling leads to a decrease in p53 activity and mitotic catastrophe in aged muscle stem cells. Cell Stem Cell 23, 544–556.e4. https://doi.org/10.1016/j.stem.2018.08.019.

35. Rust, H.L., and Thompson, P.R. (2011). Kinase consensus sequences: a breeding ground for crosstalk. ACS Chem. Biol. 6, 881–892. https://doi.org/10.1021/cb200171d.

36. Szklarczyk, D., Gable, A.L., Nastou, K.C., Lyon, D., Kirsch, R., Pyysalo, S., Doncheva, N.T., Legeay, M., Fang, T., Bork, P., et al. (2021). The STRING database in 2021: customizable protein-protein networks, and functional characterization of user-uploaded gene/measurement sets. Nucleic Acids Res. 49, D605–D612. https://doi.org/10.1093/nar/gkaa1074.

37. Rousseau, S., Morrice, N., Peggie, M., Campbell, D.G., Gaestel, M., and Cohen, P. (2002). Inhibition of SAPK2a/p38 prevents hnRNP A0 phosphorylation by MAPKAP-K2 and its interaction with cytokine mRNAs. EMBO J. 21, 6505–6514. https://doi.org/10.1093/emboj/cdf639.

38. Wang, L.S., Li, L., Li, L., Chu, S., Shiang, K.D., Li, M., Sun, H.Y., Xu, J., Xiao, F.J., Sun, G., et al. (2015). MicroRNA-486 regulates normal erythropoiesis and enhances growth and modulates drug response in CML progenitors. Blood 125, 1302–1313. https://doi.org/10.1182/blood-2014-06-581926.

39. Provatopoulou, X., Georgiou, G.P., Kalogera, E., Kalles, V., Matiatou, M.A., Papapanagiotou, I., Sagkriotis, A., Zografos, G.C., and Gounaris, A. (2015). Serum irisin levels are lower in patients with breast cancer: association with disease diagnosis and tumor characteristics. BMC Cancer 15, 898. https://doi.org/10.1186/s12885-015-1898-1.

40. Szaroszyk, M., Kattih, B., Martin-Garrido, A., Trogisch, F.A., Dittrich, G.M., Grund, A., Abouissa, A., Derlin, K., Meier, M., Holler, T., et al. (2022). Skeletal muscle derived Musclin protects the heart during pathological overload. Nat. Commun. 13, 149. https://doi.org/10.1038/s41467-021-27634-5.

41. Miyazaki, T., Otani, K., Chiba, A., Nishimura, H., Tokudome, T., Takano-Watanabe, H., Matsuo, A., Ishikawa, H., Shimamoto, K., Fukui, H., et al. (2018). A new secretory peptide of natriuretic peptide family, osteocrin, suppresses the progression of congestive heart failure after myocardial infarction. Circ. Res. 122, 742–751. https://doi.org/10.1161/CIRCRESAHA.117.312624.

42. Wissing, E.R., Boyer, J.G., Kwong, J.Q., Sargent, M.A., Karch, J., McNally, E.M., Otsu, K., and Molkentin, J.D. (2014). P38alpha MAPK underlies muscular dystrophy and myofiber death through a Bax-dependent mechanism. Hum. Mol. Genet. 23, 5452–5463. https://doi.org/10.1093/hmg/ddu270.

43. Reynolds, J.G., McCalmon, S.A., Donaghey, J.A., and Naya, F.J. (2008). Deregulated protein kinase A signaling and myospryn expression in muscular dystrophy. J. Biol. Chem. 283, 8070–8074. https://doi.org/10.1074/jbc.C700221200.

44. Yucel, N., Chang, A.C., Day, J.W., Rosenthal, N., and Blau, H.M. (2018). Humanizing the mdx mouse model of DMD: the long and the short of it. NPJ Regen. Med. 3, 4. https://doi.org/10.1038/s41536-018-0045-4.

45. Nguyen, Q., Lim, K.R.Q., and Yokota, T. (2019). Current understanding and treatment of cardiac and skeletal muscle pathology in laminin-alpha2 chain-deficient congenital muscular dystrophy. Appl. Clin. Genet. 12, 113–130. https://doi.org/10.2147/TACG.S187481.

46. Bullard, S.A., Seo, S., Schilling, B., Dyle, M.C., Dierdorff, J.M., Ebert, S.M., DeLau, A.D., Gibson, B.W., and Adams, C.M. (2016). Gadd45a protein promotes skeletal muscle atrophy by forming a complex with the protein kinase MEKK4. J. Biol. Chem. 291, 17496–17509. https://doi.org/10.1074/jbc.M116.740308.

47. Pescatori, M., Broccolini, A., Minetti, C., Bertini, E., Bruno, C., D'Amico, A., Bernardini, C., Mirabella, M., Silvestri, G., Giglio, V., et al. (2007). Gene expression profiling in the early phases of DMD: a constant molecular signature characterizes DMD muscle from early postnatal life throughout disease progression. FASEB J. 21, 1210–1226. https://doi.org/10.1096/fj.06-7285com.

48. Wei, N., Cheng, Y., Wang, Z., Liu, Y., Luo, C., Liu, L., Chen, L., Xie, Z., Lu, Y., and Feng, Y. (2015). SRSF10 plays a role in myoblast differentiation and glucose production via regulation of alternative splicing. Cell Rep. 13, 1647–1657. https://doi.org/10.1016/j.celrep.2015.10.038.

49. Sako, Y., Ninomiya, K., Okuno, Y., Toyomoto, M., Nishida, A., Koike, Y., Ohe, K., Kii, I., Yoshida, S., Hashimoto, N., et al. (2017). Development of an orally available inhibitor of CLK1 for skipping a mutated dystrophin exon in Duchenne muscular dystrophy. Sci. Rep. 7, 46126. https://doi.org/10.1038/srep46126.

50. Bachinski, L.L., Sirito, M., Bohme, M., Baggerly, K.A., Udd, B., and Krahe, R. (2010). Altered MEF2 isoforms in myotonic dystrophy and other neuromuscular disorders. Muscle Nerve 42, 856–863. https://doi.org/10.1002/mus.21789.

51. Carson, J.A., Hardee, J.P., and VanderVeen, B.N. (2016). The emerging role of skeletal muscle oxidative metabolism as a biological target and cellular regulator of cancer-induced muscle wasting. Semin. Cell Dev. Biol. 54, 53–67. https://doi.org/10.1016/j.semcdb.2015.11.005.

52. Wang, Z., Shang, P., Li, Q., Wang, L., Chamba, Y., Zhang, B., Zhang, H., and Wu, C. (2017). iTRAQ-based proteomic analysis reveals key proteins affecting muscle growth and lipid deposition in pigs. Sci. Rep. 7, 46717. https://doi.org/10.1038/srep46717.

53. Amaral, A.R., Brunetto, M.A., Brolio, M.P., Cima, D.S., Miglino, M.A., Santos, J.P.F., and Ambrosio, C.E. (2017). Abnormal carbohydrate metabolism in a canine model for muscular dystrophy. J. Nutr. Sci. 6, e57. https://doi.org/10.1017/jns.2017.59.

54. Petruzzelli, M., and Wagner, E.F. (2016). Mechanisms of metabolic dysfunction in cancer-associated cachexia. Genes Dev. 30, 489–501. https://doi.org/10.1101/gad.276733.115.

55. Prats-Puig, A., Ortega, F.J., Mercader, J.M., Moreno-Navarrete, J.M., Moreno, M., Bonet, N., Ricart, W., Lopez-Bermejo, A., and Fernandez-Real, J.M. (2013). Changes in circulating microRNAs are associated with childhood obesity. J. Clin. Endocrinol. Metab. 98, E1655–E1660. https://doi.org/10.1210/jc.2013-1496.

56. Al Azzouny, M.A., Behiry, E.G., Behairy, O.G., Abd Ellraouf, H.A., and Elfallah, A.A. (2021). Serum microRNA-486-5p expression in obese Egyptian children and its possible association with fatty liver. Diabetes Metab. Syndr. 15, 102258. https://doi.org/10.1016/j.dsx.2021.102258.

57. Bakr Zaki, M., Abulsoud, A.I., Elsisi, A.M., Doghish, A.S., Mansour, O.A.E., Amin, A.I., Elrebehy, M.A., Mohamed, M.Y., and Goda, M.A. (2019). Potential role of circulating microRNAs (486-5p, 497, 509-5p and 605) in metabolic syndrome Egyptian male patients. Diabetes Metab. Syndr. Obes. 12, 601–611. https://doi.org/10.2147/DMSO.S187422.

58. Lorente-Cebrian, S., Gonzalez-Muniesa, P., Milagro, F.I., and Martinez, J.A. (2019). MicroRNAs and other non-coding RNAs in adipose tissue and obesity: emerging roles as biomarkers and therapeutic targets. Clin. Sci. (Lond.) 133, 23–40. https://doi.org/10.1042/CS20180890.

59. Kim, Y.J., Hwang, S.H., Lee, S.Y., Shin, K.K., Cho, H.H., Bae, Y.C., and Jung, J.S. (2012). miR-486-5p induces replicative senescence of human adipose tissue-derived mesenchymal stem cells and its expression is controlled by high glucose. Stem Cells Dev. 21, 1749–1760. https://doi.org/10.1089/scd.2011.0429.

60. Xu, J., Li, R., Workeneh, B., Dong, Y., Wang, X., and Hu, Z. (2012). Transcription factor FoxO1, the dominant mediator of muscle wasting in chronic kidney disease, is inhibited by microRNA-486. Kidney Int. 82, 401–411. https://doi.org/10.1038/ki.2012.84.

61. Altomonte, J., Cong, L., Harbaran, S., Richter, A., Xu, J., Meseck, M., and Dong, H.H. (2004). Foxo1 mediates insulin action on apoC-III and triglyceride metabolism. J. Clin. Invest. 114, 1493–1503. https://doi.org/10.1172/JCI19992.

62. Hill, D.A., and Imbalzano, A.N. (2006). HMGN1 is dispensable for myogenesis and adipogenesis. Gene 371, 59–67. https://doi.org/10.1016/j.gene.2005.11.012.

63. Yakabe, M., Ogawa, S., Ota, H., Iijima, K., Eto, M., Ouchi, Y., and Akishita, M. (2018). Inhibition of interleukin-6 decreases atrogene expression and ameliorates tail suspension-induced skeletal muscle atrophy. PLoS One 13, e0191318. https://doi.org/10.1371/journal.pone.0191318.

64. Mammen, A.L., and Sartorelli, V. (2015). IL-6 blockade as a therapeutic approach for Duchenne muscular dystrophy. EBioMedicine 2, 274–275. https://doi.org/10.1016/j.ebiom.2015.03.018.

65. Hathout, Y., Brody, E., Clemens, P.R., Cripe, L., DeLisle, R.K., Furlong, P., Gordish-Dressman, H., Hache, L., Henricson, E., Hoffman, E.P., et al. (2015). Large-scale serum protein biomarker discovery in Duchenne muscular dystrophy. Proc. Natl. Acad. Sci. U S A 112, 7153–7158. https://doi.org/10.1073/pnas.1507719112.

66. Crescioli, C., Sottili, M., Bonini, P., Cosmi, L., Chiarugi, P., Romagnani, P., Vannelli, G.B., Colletti, M., Isidori, A.M., Serio, M., et al. (2012). Inflammatory response in human skeletal muscle cells: CXCL10 as a potential therapeutic target. Eur. J. Cell Biol. 91, 139–149. https://doi.org/10.1016/j.ejcb.2011.09.011.

67. Wright, C.R., Brown, E.L., Della-Gatta, P.A., Ward, A.C., Lynch, G.S., and Russell, A.P. (2014). G-CSF does not influence C2C12 myogenesis despite receptor expression in healthy and dystrophic skeletal muscle. Front. Physiol. 5, 170. https://doi.org/10.3389/fphys.2014.00170.

68. Zhang, C., Li, Y., Wu, Y., Wang, L., Wang, X., and Du, J. (2013). Interleukin-6/signal transducer and activator of transcription 3 (STAT3) pathway is essential for macrophage infiltration and myoblast proliferation during muscle regeneration. J. Biol. Chem. 288, 1489–1499. https://doi.org/10.1074/jbc.M112.419788.

69. Roberts, B.M., Frye, G.S., Ahn, B., Ferreira, L.F., and Judge, A.R. (2013). Cancer cachexia decreases specific force and accelerates fatigue in limb muscle. Biochem. Biophys. Res. Commun. 435, 488–492. https://doi.org/10.1016/j.bbrc.2013.05.018.

70. Acharyya, S., Butchbach, M.E., Sahenk, Z., Wang, H., Saji, M., Carathers, M., Ringel, M.D., Skipworth, R.J., Fearon, K.C., Hollingsworth, M.A., et al. (2005). Dystrophin glycoprotein complex dysfunction: a regulatory link between muscular dystrophy and cancer cachexia. Cancer Cell 8, 421–432. https://doi.org/10.1016/j.ccr.2005.10.004.

71. Talbert, E.E., Cuitino, M.C., Ladner, K.J., Rajasekerea, P.V., Siebert, M., Shakya, R., Leone, G.W., Ostrowski, M.C., Paleo, B., Weisleder, N., et al. (2019). Modeling human cancer-induced cachexia. Cell Rep. 28, 1612–1622.e4. https://doi.org/10.1016/j.celrep.2019.07.016.